AFRL-RV-PS-TP-2017-0014

AFRL-RV-PS-TP-2017-0014

AUTOMATIC NOISE-REMOVAL/SIGNAL-REMOVAL BASED ON GENERAL-CROSS-VALIDATION THRESHOLDING IN SYNCHROSQUEEZED DOMAINS, AND ITS APPLICATION ON EARTHQUAKE DATA

Annual Report

Charles A. Langston

Center for Earthquake Research and Information
University of Memphis
3876 Central Ave., Ste. 1
Memphis, TN 38152

01 April 2017

Technical Report

APPROVED FOR PUBLIC RELEASE; DISTRIBUTION IS UNLIMITED.

AIR FORCE RESEARCH LABORATORY
Space Vehicles Directorate
3550 Aberdeen Ave SE
AIR FORCE MATERIEL COMMAND
KIRTLAND AIR FORCE BASE, NM 87117-5776

DTIC COPY

NOTICE AND SIGNATURE PAGE

AFRL-RV-PS-TP-2017-0014 HAS BEEN REVIEWED AND IS APPROVED FOR PUBLICATION IN ACCORDANCE WITH ASSIGNED DISTRIBUTION STATEMENT.

//SIGNED//	//SIGNED//
Dr. Frederick Schult Program Manager, AFRL/RVBYE	Dr. Thomas R. Caudill, Acting Chief AFRL Battlespace Environment Division

REPORT DOCUMENTATION PAGE

Form Approved OMB No. 0704-0188

1. REPORT DATE *(DD-MM-YYYY)*
01-04-2017

2. REPORT TYPE
Technical Report

3. DATES COVERED *(From - To)*
01 Mar 2016 – 28 Feb 2017

4. TITLE AND SUBTITLE
Automatic Noise-Removal/Signal-Removal Based on General-Cross-Validation Thresholding in Synchrosqueezed Domains, and its Application on Earthquake Data
Annual Report

5a. CONTRACT NUMBER
FA9453-16-C-0015

5b. GRANT NUMBER

5c. PROGRAM ELEMENT NUMBER
62601F

6. AUTHOR(S)
Charles A. Langston

5d. PROJECT NUMBER
1010

5e. TASK NUMBER
PPM00019641

5f. WORK UNIT NUMBER
EF128703

7. PERFORMING ORGANIZATION NAME(S) AND ADDRESS(ES)
Center for Earthquake Research and Information
University of Memphis
3876 Central Ave., Ste. 1
Memphis, TN 38152

8. PERFORMING ORGANIZATION REPORT NUMBER

9. SPONSORING / MONITORING AGENCY NAME(S) AND ADDRESS(ES)
Air Force Research Laboratory
Space Vehicles Directorate
3550 Aberdeen Avenue SE
Kirtland AFB, NM 87117-5776

10. SPONSOR/MONITOR'S ACRONYM(S)
AFRL/RVBYE

11. SPONSOR/MONITOR'S REPORT NUMBER(S)
AFRL-RV-PS-TP-2017-0014

12. DISTRIBUTION / AVAILABILITY STATEMENT
Approved for public release; distribution is unlimited (OPS-17-13268 dtd 06 Jun 2017)

13. SUPPLEMENTARY NOTES

14. ABSTRACT
Recorded seismic signals are often corrupted by noise. An automatic noise attenuation method for single-channel seismic data is presented, based upon high-resolution time-frequency analysis. Synchrosqueezing is a time-frequency reassignment method aimed at sharpening a time–frequency picture. Noise can be distinguished from the signal and attenuated more easily in this reassigned domain. The threshold level is estimated using a general cross validation approach that does not rely on any prior knowledge about the noise level. Efficiency of thresholding has been improved by adding a pre-processing step based on Kurtosis measurement and a post-processing step based on adaptive hard thresholding. The proposed algorithm can either attenuate the noise (either white or colored) keeping the signal or remove the signal and keep the noise. Hence, it can be used in either normal denoising applications or pre-processing in ambient noise studies. We test the performance of the proposed method on synthetic, microseismic, and earthquake seismograms.

15. SUBJECT TERMS
signal analysis, filtering, time-frequency representations, noise removal, continuous wavelet transform, synchrosqueezing

16. SECURITY CLASSIFICATION OF:			17. LIMITATION OF ABSTRACT	18. NUMBER OF PAGES	19a. NAME OF RESPONSIBLE PERSON
					Dr. Frederick Schult
a. REPORT	b. ABSTRACT	c. THIS PAGE			19b. TELEPHONE NUMBER *(include area code)*
Unclassified	Unclassified	Unclassified	Unlimited	44	

Standard Form 298 (Rev. 8-98)
Prescribed by ANSI Std. 239.18

This page is intentionally left blank.

Table of Contents

List of Figures

1. SUMMARY

This work has culminated in 4 publications concerning Time-Frequency Representations of seismic data and resulted in experimental software that has been delivered to AFRL. The basic idea behind all techniques involves manipulation of a two-dimensional mapping where the location of a “signal” is discriminated from “noise” on a plane consisting of complex amplitudes determined from the transform of a short time window of seismic data. A common transform is the short time window Fourier transform (STFT) but other transforms, such as the continuous wavelet transform (CWT) and the synchrosqueezed CWT may represent the time series data in more compact form (Figure 1). The STFT is the basis for the common spectrogram where short running time windows of the data are Fourier transformed and then the amplitude or power spectra are plotted as a function of time. The CWT may be implemented with a choice of different wavelet functions and is computed in a similar manner to the STFT in which a short time window is transformed with wavelet coefficients at different scales being plotted against time. The synchrosqueezed CWT (SS-CWT) represents another processing step where, as shown in Figure 1, the CWT is modified by assigning the energy of closely adjacent wavelet coefficients to ridges in the CWT time-scale map. Both the CWT and the SS CWT attempts to represent the seismic signal (and the noise) by the smallest number of coefficients.

The transformed signal can be manipulated by a number of techniques to characterize both signal and noise and then remove either. Once a quantitative characterization is obtained for properties of the noise, it can be removed by applying a threshold criterion to sections of the Time-scale map. The processed Time-scale map is then inverse transformed to obtain the denoised signal.

In Mousavi et al. (2016a), an algorithm was developed around the SS-CWT for the purpose of detecting microtremors within noise. In this algorithm, the time-scale CWT map for small events embedded in noise was partitioned based on the character of high scale (low frequency) background noise and low scale (high frequency) microtremors. This part is most analogous to highpass filtering where the higher frequency part of the map is treated separately from the low frequency part. Assumptions involve considering an event to be localized at small scales and in time and to have larger wavelet coefficient amplitudes. Noise is characterized by low values of wavelet coefficients but by larger numbers of coefficients. After determining the boundary of the high scale noise and low scale signals, the map is split and synchrosqueezed to reduce the number of wavelet coefficients needed to describe both the noise and the signal. Using a pre-event time window, the statistics of the noise in the signal and noise parts of the map is determined. Using these statistics, “soft-thresholding” is applied to the high scale noise segment and the noise attenuated across scale by dividing by the high amplitude wavelet coefficients. A detection function is then constructed to detect the high amplitude signal components by computing the energy from a Parseval-type computation of the wavelet coefficients as a function of time.

Block thresholding was explored by Mousavi and Langston (2016a) incorporating only the signal’s CWT. First the CWT time-scale map is computed for a time series.

Gaussian noise is then detected in the CWT through computation of the kurtosis (HOS or higher order statistics). This noise is then removed from the CWT map by a statistical test. The data are then processed scale by-scale as a function of time by determining an optimum time block length using an estimate of the strength of the signal's wavelet coefficients compared to the noise. The "hybrid" aspect of this process is having different block lengths for the coefficients at each scale and attenuating wavelet coefficients based on adaptive parameters that change with time and scale. The attenuated noise coefficients are then subject to an additional Weiner filter and transformed back into the time domain. Remarkably, all of these wavelet coefficient manipulations preserve relative amplitudes and particle motions of seismic phases in the three component data. Use of the CWT is relatively computationally intensive in these previous techniques compared to a STFT.

Mousavi and Langston (2016b) incorporated the STFT to compute the time-frequency map and then applied an adaptive block size and threshold value to remove the noise. Noise level is estimated by assuming that the signal is larger than the noise and by tracking minima on the time-frequency plane. There is an arcane recursive process for determining the noise variance in one section of the plane compared to adjacent sections. Once the statistics of the noise is known, the Fourier coefficients of the noise in one block can be attenuated by using the noise estimates in adjacent blocks. The denoised STFT is then transformed back into the time domain. Although this method does not preserve waveform as well as the previous methods, it is almost 2 orders of magnitude faster in computation time and is appropriate for fast detection algorithms.

The remainder of this annual report concerns our work in putting together many of the previously explored techniques in the first 3 papers with the idea of general-cross-validation thresholding (GCV). GCV takes advantage of the distilling effect of the SS-CWT to reduce the areal density of CWT coefficients on the complex time-frequency plane. Using these techniques one can then remove noise from signal or signal from noise. This latter characteristic offers a way to pre-process ambient seismic noise to remove unwanted impulsive earthquake signals before applying correlation to obtain the Green's function between 2 seismic stations.

2. INTRODUCTION

During the acquisition process, seismic data are often corrupted by noise. Seismic denoising aims at increasing the signal-to-noise ratio (SNR) by eliminating this additive noise through some signal processing steps, while preserving important features of the seismic signal. Spectral filtering, as a common approach for improving the SNR, is not effective for suppressing noise that has the same frequency content as the signal. Moreover, it can distort the signal (Douglas 1997) and/or generate artifacts prior to impulsive arrivals (Scherbaum 2001).

A more effective noise suppression can be achieved through thresholding methods in time-frequency domains; such as using the S-transform (Pinnegar and Eaton, 2003; Schimmel and Gallart, 2007; Parolai 2009; Ditommaso et al., 2010, 2012; Tselentis et al., 2012), radon transform (Sabbione et al., 2013, 2015; Zhang et al., 2015), the wave packet transform (Galiana-Merino et al, 2003; Shuchong and Xun, 2014), f-x or f-k filtering (Bekara and van der Baan, 2009; Naghizadeh 2011; Naghizadeh and Sacchi, 2012; Chen and Ma, 2014), singular spectrum analysis (Oropeza and Sacchi, 2011), sparse transform based denoising (Chen et al., 2016), a mathematical morphology based denoising approach (Li et al., 2016), reduced-rank filtering (Velis et al., 2015), damped multichannel singular spectrum analysis (Huang et al., 2016), the non-local means (NLM) algorithm (Bonar and Sacchi 2012) or the continuous wavelet transform (Pazos et al., 2003; Sobolev and Lyubushin, 2006; Mousavi and Langston, 2016a, 2016c).

Bekara and van der Baan, (2009), Han and Van Der Baan, (2015), Gomez and Velis (2016) showed that seismic noise can be removed effectively using empirical mode decomposition (EMD). EMD (Huang et al. 1998) is a data driven time-frequency analysis technique that adaptively decomposes a signal into a set of localized, modulated oscillations termed intrinsic mode functions (IMFs).

Recently, a new reassignment technique termed synchrosqueezing (SS) was introduced as a powerful alternative to EMD (Daubechies et al 2011). SS produces a sharpened time-frequency representation (TFR) of the signal that highly localizes modulated oscillations. It has better mathematical support, and adaptability properties compared to EMD (Thakur et al. 2013; Herrera et al. 2014; Herrera et al. 2015).

Meignen et al. (2012) and Ahrabian and Mandic, (2015) have introduced denoising techniques based on synchrosqueezing for univariate and multivariate signals respectively. These methods are based on identifying common modulated oscillations in elements of data. They outperformed wavelet and EMD based methods. Mousavi et al., (2016a) showed that a simple normalization step in the synchrosqueezed domain can improve the SNR of microseismic events.

Here we introduce an adaptive and fast algorithm for automatic noise or signal removal based on the synchrosqueezed-continuous wavelet transform (SS-CWT), incorporating higher-order statistics (HOS), general cross validation (GCV), and wavelet hard-thresholding (WHT) for seismic data. The proposed method takes advantage of the mode decomposition property of the SS-CWT. Major components present in recorded data are thresholded separately based on data characteristics. Synthetic and real simulations show that the proposed method is effective for accurate denoising and increasing the SNR of microseismic and OBS data, as well as filtering out the seismic signal in the case of noise studies.

3. TECHNICAL APPROACH

3.1. Theoretical Background

3.1.1. Time-Frequency Representation (TFR)

We assume that real signals can be modeled by time-varying oscillatory components defined as (Herrera et al. 2014):

$$s(t) = A(t)\cos\left(2\pi\phi(t)\right) \quad , \tag{1}$$

where $\phi(t)$ and *A(t)* are the instantaneous phase and amplitude of a time series *s(t)* respectively. The derivative of the instantaneous phase is referred to as instantaneous frequency $f=\frac{1}{2\pi}\frac{\partial\phi(t)}{\partial t}$. In order to identify the associated *A(t)* and $\phi(t)$ for a given signal *y(t)*, the Hilbert transform can be used to generate the analytic signal (Gabor 1946).

$$y_{+}^{a}(t)=y(t)-iH\left[y(t)\right], \tag{2}$$

where *H[ ]* is the Hilbert transform. The analytic signal is complex and can be used to find the *A(t)* and $\phi(t)$.

However, real-world signals like seismic traces usually consist of many components and are generally contaminated with noise. Hence, the recorded signal can be represented as a combination of components plus some additive noise $\varepsilon(t)$:

$$y(t)=\sum_{k=1}^{K}s_k(t)+\sigma\varepsilon(t)=\sum_{k=1}^{K}A_k(t)\cos\left(2\pi\phi_k(t)\right)+\sigma\varepsilon(t) \quad , \tag{3}$$

where, *K* is the number of components in the recorded signal and σ is the noise level. Therefore the analytic signal represents a mixture of the amplitudes and phases of individual components of the observed seismic traces. Time-frequency transforms (TFT) aim to localize individual oscillatory components of the recorded signals. The non-stationary nature of seismic signals indicates that instead of considering a signal in the frequency or time domain (one dimensional), it is often more informative to study their TFR. The two dimensional evolution of the spectral content of the seismic data can be tracked in a TFR.

The advantage of denoising in a time-frequency domain over traditional spectral filtering is that it allows for separating the noise from the signal even in the same pass band as long as they are temporally separated.

Many TFTs exist for this purpose such as short time Fourier transform (STFT) and continuous wavelet transform (CWT). A comprehensive review and comparison of application of different TFTs on seismic data can be found in Tary et al. (2014). Here, we just give a short description of STFT, and CWT to briefly address resolution problems and the enhancement achieved by the synchrosqueezing step.

3.1.2. Short Time Fourier Transform (STFT)

The Fourier transform decomposes a signal into sine and cosine basis functions. The most common TFT used for time–frequency analysis is the STFT (also known as the windowed Fourier transform) (Gabor 1946; Allen and Rabiner 1977). Indeed, the STFT is the Fourier transform of successive windows of the signal:

$$F_y(\tau,\xi)=\int_{-\infty}^{+\infty}y(t)G(t-\tau)e^{-i\xi t}dt \quad , \tag{4}$$

where, *t* is the time, ξ is angular frequency, τ is time delay, and *G(t)* is a chosen window function which is usually either a Gaussian or Hann function. The sliding window is held constant during the analysis irrespective of investigated frequencies. Thus, both time and frequency resolutions are kept constant and depend directly on the window size (Reine et al. 2009). Tary et al. (2014) define time and frequency resolutions as the ability to distinguish two wavefronts and two spectral peaks respectively. However, these resolutions are always limited by the Heisenberg/Gabor uncertainty principle (Gabor 1946; Mallat 1999) i.e. $\Lambda_t \Lambda_f \geq 4\pi$ where Λ_t represents the time resolution and Λ_f stands for the frequency resolution.

TFR resolution obtained from any transform depends on both intrinsic characteristics of the analyzed signal and on specific properties of the chosen transform, hence the TFT should be viewed as a measurement device (Auger et al. 2013).

This time-frequency trade off and the fixed resolution of the STFT imply that one will lose time resolution (accurate timing of frequency changes) if one wants to accurately identify spectral peaks (high-frequency resolution) (Tary et al., 2014).

3.1.3. Continuous Wavelet Transform (CWT)

Multi-resolution transforms such as the CWT (Daubechies and Heil (1992) can obtain a better TFR for signals with both low and high frequency content, since the signal is analyzed under different resolutions (or scales) at different frequencies. CWT is accomplished through a prototype analyzing function known as the mother wavelet ψ, which can be interpreted as a bandpass. The CWT of y in equation (5.3) at scale a and time shift τ is given by: (Daubechies and Heil (1992); Mallat, 1999)

$$W_y(a,\tau) = \langle y, \psi_{a,\tau} \rangle = \int_{-\infty}^{+\infty} y(t) a^{-\frac{1}{2}} \psi^* \left(\frac{t-\tau}{a} \right) dt \quad , \tag{5}$$

in which, * denotes the complex conjugate, $\langle y, \psi_{a,\tau} \rangle$ is the inner product, and W_y is the coefficient representing finite energy of the signal y in a concentrated time–frequency picture. The mother wavelet ψ, should be a square integrable function in which its Fourier transform $\hat{\psi}(\xi)$, should vanish at zero frequency:

$$\hat{\psi}(0) = \int \psi(t) dt = 0 \quad . \tag{6}$$

This is called the admissibility condition (Farge, 1992; Daubechies and Heil, 1992). According to Plancherel's theorem, equation (5) can be written in the frequency domain as: (Daubechies et al. 2011; Herrera et al. 2014)

$$W_y(a,\tau) = \frac{1}{2\pi} \int_{-\infty}^{+\infty} \hat{y}(\xi) a^{-\frac{1}{2}} \hat{\psi}^*(a\xi) e^{i\xi\tau} d\xi \ , \tag{7}$$

where, $\hat{y}(\xi)$ is the Fourier transform of the signal. The inversion of the CWT can be expressed as:

$$y(t)=\frac{1}{C_\psi}\iint W_y(a,\tau)d\tau\frac{da}{a^2}\,, \tag{8}$$

where, the constant C_ψ is given by: (Thakur et al. 2013)

$$C_\psi=\int_0^\infty \xi^{-1}\hat{\psi}^*(\xi)d\xi \quad . \tag{9}$$

The CWT can be thought of as the cross–correlation of y with stretched (or compressed) and shifted mother wavelets, to capture oscillatory features of the signal at different frequencies. The variable length of ψ leads to a flexible trade-off between frequency and time-localization compared to the STFT (Tary et al., 2014). However, it still displays spectral smearing due to the finite size of the operator (Hall 2006).

3.1.4. Synchrosqueezing

Synchrosqueezing (SS) is a relatively new technique introduced by Daubechies and Maes (1996) and Daubechies et al. (2011) as a powerful tool for precisely decomposing and analyzing a signal. It can be classified as a time-frequency reassignment method aiming at a sharpened TFR by applying a post-processing reallocation on the original time-frequency representation. However, unlike classical reassignment methods (e.g. Auger and Flandrin 1995; Chassande-Mottin et al. 1997), SS is adaptive to different types of data, visually informative, and enjoys a simple and efficient reconstruction formula (Yang 2015).

At each time or space location, the SS process reassigns values of the TFR based on their local oscillation. The idea behind SS is that concentrating a spectrogram's energy around instantaneous frequencies will decrease spectral smearing, and thus sharpening the TFR, while still allowing its reconstruction. SS can be used to enhance many classical TFRs e.g. the synchrosqueezed continuous wavelet transform (SS-CWT) as in (Daubechies et al. 2011; Thakur et al. 2013; Iatsenko et al. 2015), the synchrosqueezed short time Fourier transform (SS-STFT) as in (Thakur and Wu 2011; Iatsenko et al. 2015), the synchrosqueezed wave packet transform (SS-WPT) as in (Yang 2015), the synchrosqueezed curvelet transform (SS-CT) as in (Yang and Ying 2014), and the synchrosqueezed S-transform (SS-ST) as in (Huang et al. 2015).

It has been shown that compared to the STFT and CWT, the SS-CWT has superior frequency resolution for distinguishing oscillatory components of complicated signals (Thakur et al. 2013). Rigorous analysis has proven the stability and robustness of synchrosqueezing for analyzing 1D signals corrupted by noise or perturbations in the signal (Thakur et, al., 2013).

Following Daubechies et al. (2011) the SS-CWT is performed in three steps. First, wavelet coefficients $W_y(a,\tau)$, of the recorded signal y, are calculated i.e. using (5) or (7). In the next step, a candidate instantaneous frequency $\omega_y(a,\tau)$ can be computed for wavelet coefficients of y at any point (a,τ) as:

$$\omega_y(a,\tau) = -\frac{i}{2\pi W_y(a,\tau)} \frac{\partial W_y(a,\tau)}{\partial t} \text{, for } W_y(a,\tau) \neq 0. \tag{10}$$

The instantaneous frequencies are known as ridges in the TFR (Auger et al. 2013). In practice the very small wavelet coefficients $W_y(a,\tau)$ need to be removed to make the division operator numerically stable. SS squeezes the energy around these ridges (condensing the CWT coefficients at each time point along the scale axis) to decrease the smearing. To do this, in the last step, the information from the time-scale plane is transformed to the time-frequency plane, $(a,\tau) \rightarrow \langle \omega_y(a,\tau), \tau \rangle$. This operation is called synchrosqueezing and has been shown to improve the concentration of energy and, as a result, readability of the TFR (Daubechies et all. 2011). If the number of scales used in the CWT and the sampling frequency are N and *sf* respectively, frequencies on the SS-CWT would be $\omega_\ell = \ell sf/N$, $\ell \in [1,N]$ because $W_y(a,\tau)$ is calculated at discrete values a_k. The CWT coefficients within the frequency range $\Delta\omega = \omega_\ell - \omega_{\ell-1} = sf/N$, will be added up to the center frequency ω_ℓ to construct each instantaneous frequency. Hence, the synchrosqueezed transform is defined as:

$$T_y(\omega_\ell, \tau) = \Delta\omega^{-1} \sum_{a_k | \omega(a_k,\tau) - \omega_\ell | \leq \Delta\omega/2} W_y(a_k,\tau) a_k^{-3/2} \Delta a_k \quad , \tag{11}$$

where ω_ℓ is the ℓth discrete frequency, a_k is the *k* th scale, and $\Delta a = a_k - a_{k-1}$. We can recover individual components y_k, from the T_y by integrating the coefficients over frequencies ω_ℓ, that correspond to the k_{th} component. Following (Thakur et al. 2013) let the $l \in L_k(t)$ a small frequency band around the ridge of k_{th} component in the SS-CWT. This band can be estimated using a standard least-square ridge extraction method (e.g. Carmona, et al., 1997) or defined manually. Because y_k is real, then we will have:

$$y_k(t) = 2C_\psi^{-1} \Re e\left(\sum_{l \in L_k(t)} T_y(\omega_\ell, t) \right). \tag{12}$$

Doing so, one can decompose a signal into its constituent components. It is clear that the highly structured TFR provided by synchrosqueezing (Figure 1) can be exploited for classical signal processing applications such as the denoising (Auger et al. 2013).

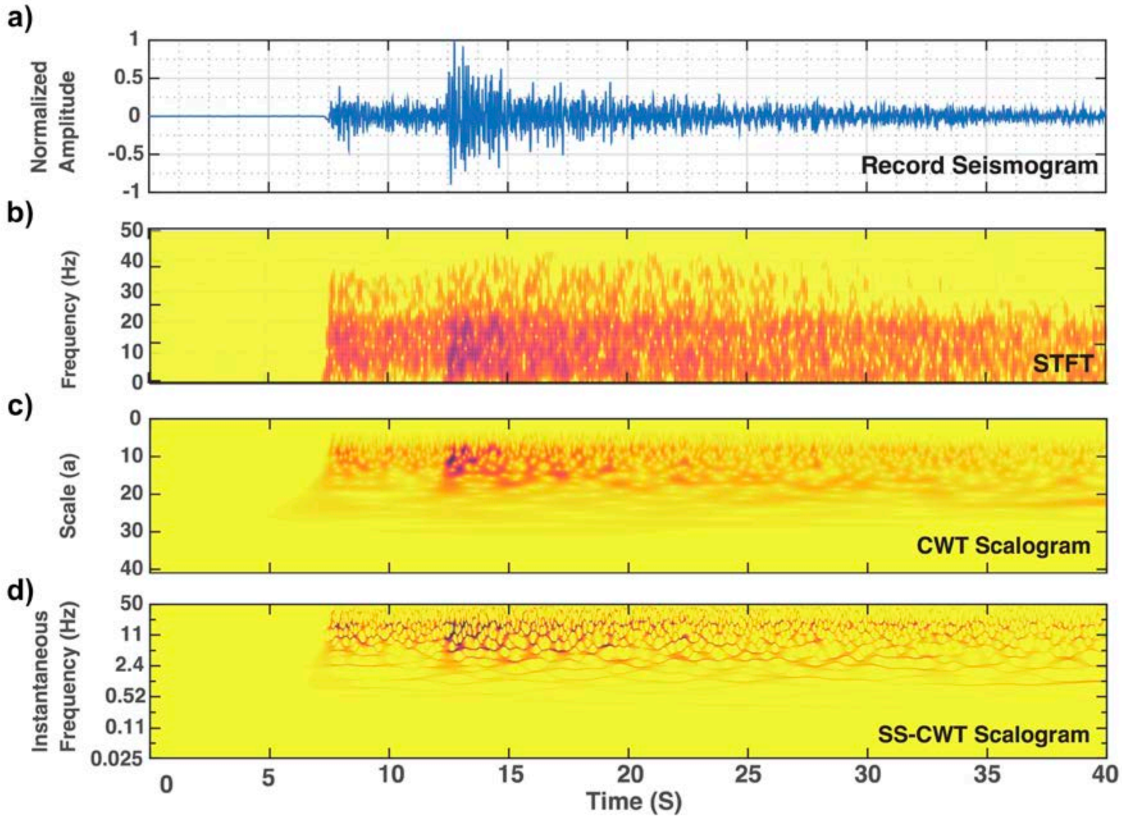

Figure 1. The top panel shows a high SNR vertical component accelerogram for a M3.5 event recorded at station HALT, TN, in the New Madrid Cooperative Seismic Network. The next panels downward show the STFT, CWT, and SS-CWT, respectively, representing TFRs of the same signal. *The variable length of* ψ *leads to a relatively higher time-frequency resolution of CWT (c) compared to the STFT (b). However, it still displays spectral smearing due to the finite size of the operator. Note the sharpened TFR obtained by the SS-CWT (d).*

3.1.5. Time-Frequency Denoising

Recalling the model in (3) for the recorded data (observation) *y*, the goal of denoising is to remove as much of the additive noise ε as possible, while preserving the main features of the signal of interest *s* where, for arguments sake, we have dropped the subscript *k*. Hence, the denoising problem can be viewed as a nonparametric regression problem and any denoising algorithm can be thought of as an operator *D* that maps the noisy data *y* onto an estimate of the signal of interest $\tilde{s} = D(y)$. The precision of the estimate is measured by the expected squared error:

$$R(\tilde{s} - s) = E\|\tilde{s} - s\|_2^2 \quad , \tag{13}$$

Donoho and Johnstone, (1994, 1995) in their pioneering work showed that nonlinear thresholding estimators operating in the wavelet domain achieve nearly minimax risk over a large class of functions that cannot be improved upon over an order of magnitude by any other estimator (Johnstone and Silverman, 1997). This is based on the energy compaction or the sparsity property of the wavelet transform, which can concentrate the signal's energy into a few large magnitude coefficients, while the small coefficients are more likely to be associated with the noise. Hence, noise power can be suppressed by selecting a suitable threshold level λ, and thresholding rule η. The simplest but still most popular thresholding rules are hard and soft thresholding, respectively, given by:

$$\eta_\lambda^h\left(W_y\right) = W_y\, I\left(\left|W_y\right| > \lambda\right) \ , \tag{14}$$

and

$$\eta_\lambda^s\left(W_y\right) = \mathrm{sgn}\left(W_y\right)\left(\left|W_y\right| - \lambda\right) \ , \tag{15}$$

where sgn(.) is the sign function and W_y are the wavelet coefficients of observation *y*.

3.2. The Proposed Method

In our previous study (Mousavi and Langston, 2016a), we showed that the efficiency of denoising for seismic data can be significantly improved by hybrid approaches that incorporate pre-processing, thresholding and post-processing steps. Following this strategy our denoising approach in the SS-CWT domain is proposed as follows.

3.2.1. Pre-Processing

In this step, after transforming the observed data y, into the CWT domain, scales, which purely consist of coefficients associated to the Gaussian noise, are detected and removed from the TFR using the HOS and Kurtosis criteria, leaving the scales with a combination of noise and signal. The kurtosis, *kurt*, of N observed coefficients W_y, is calculated by: (Bickel and Doksum, 1977)

$$kurt_y = \frac{\sum_{n=1}^{N}\left(W_{y_n} - \mu_{W_y}\right)^4}{N\sigma_{W_y}^4} - 3 \, , \tag{16}$$

where σ_{W_y} and μ_{W_y} are, respectively, the estimated standard deviation and mean of wavelet coefficients W_y. The HOS criterion for distinguishing a Gaussian distribution from a non-Gaussian distribution then is defined by:

$$\left|kurt_y\right| \leq \frac{\sqrt{24/N}}{\sqrt{1-\alpha}}, \tag{17}$$

where α is the level of confidence. Ravier and Amblard, (2001) numerically estimated an optimum value for α, as 90%. This process acts as the equivalent of an automatic band-pass filter and removes noise with lower and higher frequency content compared to the frequency range of seismic signals. This step improves wavelet thresholding results by removing high-power coherent noise (usually associated with colored noise), outside of the frequency range of the seismic signal, from the time-frequency representation of data.

3.2.2. General Cross Validation Thresholding

The pre-processed coefficients then are processed to obtain SS-CWT coefficients T_y using (11). Major oscillatory components of the signal represented by coefficients in a narrow frequency band along the ridges are then thresholded using Donoho's hard-thresholding scheme, (14). This is based on the widely accepted idea that noise is best characterized across the instantaneous frequencies (Ahrabian and Mandic 2015). The optimal threshold level λ_{ij} is automatically determined using the general cross validation (GCV) approach, proposed and developed by Nason (1996), and Weyrich and Warhola (1995), for each component (ridge). General cross-validation (GCV) is used in the statistics as an automatic procedure for selecting optimal smoothing parameters. In the GCV procedure, a data point is systematically excluded from the construction of an estimate, and then the value of excluded data point is predicted and compared with the true value. Following Jansen et al., (1997) the GCV function is defined as:

$$GCV(\lambda) = \frac{1}{N} \frac{\left\| T_y - \tilde{T}_\lambda \right\|^2}{\left\| \frac{N_0}{N} \right\|^2} \quad , \tag{18}$$

where, the $\tilde{T}_\lambda$ are thresholded coefficients using a threshold value of λ, and N_0 is the number of coefficients that would be zeroed using the threshold value λ. This function mimics the errors between the estimation and true signal hence its minimum can be used to select an optimal threshold value. The equation (18) is only a function of λ, and does not rely on any noise level estimation, which is not a trivial task in the synchrosqueezed domain. Jansen et al., (1997) showed that threshold values determined by finding the minimum of the GCV, are asymptotically optimal and minimize the mean square error R. A grid search or minimization procedure such as Fibonacci search then can be used to find the optimal threshold λ_0 producing a minimum GCV. Thresholding major components of the signal in this manner provides a fast and effective method for increasing the localization of the TFR and obtains an initial estimate of the signal using the inverse transform in (12).

3.2.3. Post-Processing

Similar to (Ghael et al. 1997) signal estimation is improved with a post-processing step by applying a simple level-dependent, wavelet threshold on the signal obtained from the previous step. For this, the initial estimate of the seismic signal is CWT transformed again and coefficients at all scales are thresholded using the hard-thresholding rule, scale-by-scale. In this step the threshold value is estimated using the universal threshold of (Donoho and Johnstone 1994):

$$\lambda = \sigma_n \sqrt{2 \ln N} \quad , \tag{19}$$

where the variance of the noise, σ_n^2, is estimated in each scale from the median of wavelet coefficients prior to the signal's arrival $\sigma_n = median\left(\left|W_y\right| \le \lambda\right) / 0.6745$. The final estimate of the denoised seismic signal, $\tilde{s}$, is obtained by applying the inverse CWT transform, i.e. (8), over the thresholded coefficients.

Using the hard thresholding scheme makes it easy to implement the method in a reverse manner to remove the signal's energy and keep the noise.

$$\eta_\lambda^{hR}\left(W_y\right) = \lambda\, I\left(\left|W_y\right| \le \lambda\right) \quad . \tag{20}$$

The latter will have application in the ambient noise studies.

4. RESULTS AND DISCUSSION

The algorithm is applied to one synthetic and three field seismograms. In our implementation of the CWT and SS-CWT, we use a Morlet wavelet as the mother wavelet with 100 scales. Approximate arrival times are determined manually. However this can be automated using any automatic onset picker in the wavelet domain such as those proposed by Karamzadeh et al, (2013), Bogiatzis and Ishii, (2015) or Mousavi et al. (2016a). SNR is measured as the root mean square amplitude in a time window around the signal to a same length window of preceding noise.

4.1. Synthetic Data

A local synthetic seismogram and its contaminated versions with random and real seismic noise (Figure 2) with a SNR of 2.5 are used for the synthetic test. The synthetic seismogram is calculated using the frequency wavenumber method (Zhu and Rivera, 2002). A point source was located at a depth of 12 km, and three component seismograms were computed for a receiver located \on the surface at an epicentral distance of 80 km. Real seismic noise recorded by the New Madrid Cooperative Seismic Network was added to the synthetic seismogram in a way to yield to SNR of 2.5 for the resulting seismogram (Figure 2).

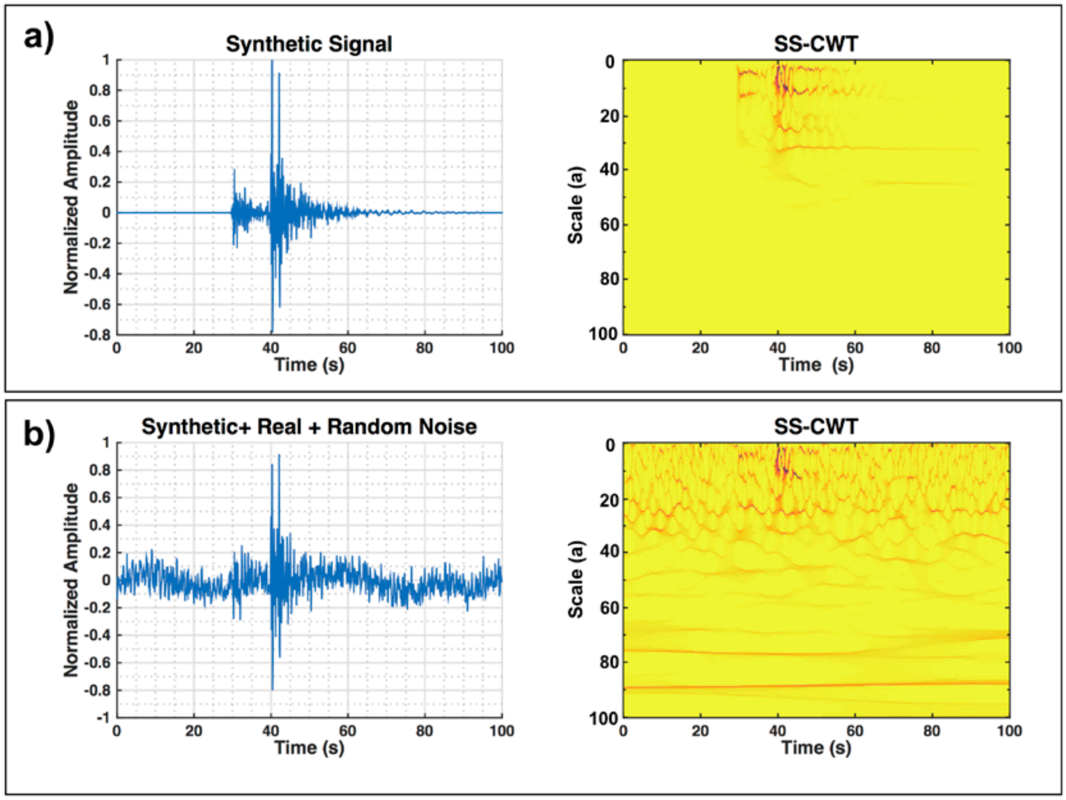

Figure 2. This figure illustrates the process of adding noise to the synthetic seismogram. *Each panel shows the annotated time series with its associated SS-CWT. The resulting noisy seismogram contains both long-period and broadband stochastic noise signals.*

Effects of each step on the noisy trace are presented in Figure 3. The pre-processing step removes those decomposition levels that purely consist of the noise. Hence, it acts like an automatic band pass filtering (Figure 3a). In the GCV thresholding step noisy coefficients are attenuated and a more distinct representation of noise and signal is provided (Figure 3b). In the post-processing step, the isolated noisy coefficients remaining after the previous steps are cleaned up (Figure 3c). The denoised and original signal are presented in Figure 4.

The method was successful in removing the random noise and improving the SNR. The denoised and synthetic signals match very well over the entire waveform (Figure 4a) except at the very beginning of the P arrival and end of the P coda. Polarity and amplitude of the first two cycles of the P arrival are preserved very well, however, a very small time shift (less than one sample interval) exists between the denoised and synthetic signals (Figure 4a). The P wave arrival which was buried under the noise became clear after the denoising. This can improve arrival time picking and as a result the source location estimation. However, P coda is smoothed at the very end. The algorithm is also very successful in removing the seismic energy from the waveform (Figure 4b). Comparing scalograms in Figures 4a and 4b, the seismic energy between 30 to 50 s has been removed from the data without changing the time-frequency structure of the background noise in the surrounding areas.

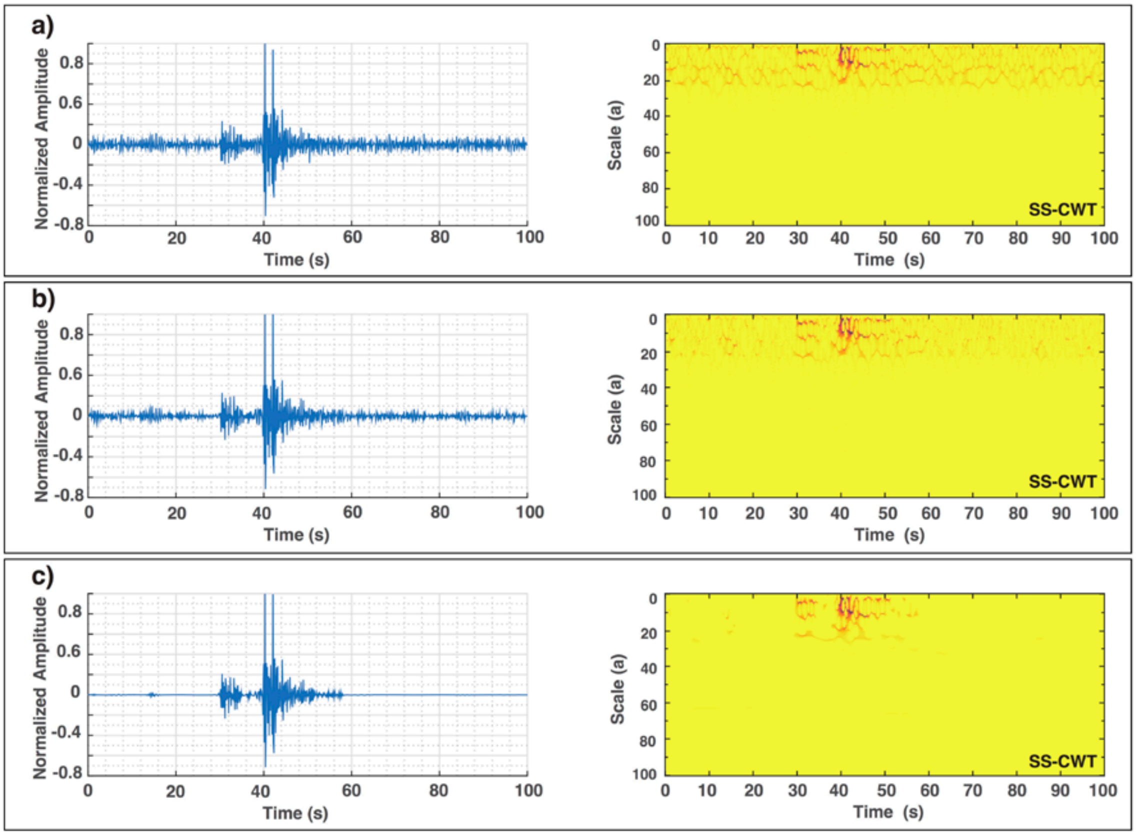

Figure 3. This figure illustrates the noisy synthetic after the pre-processing (a), GCV-thresholding (b), and post-processing (c) steps.

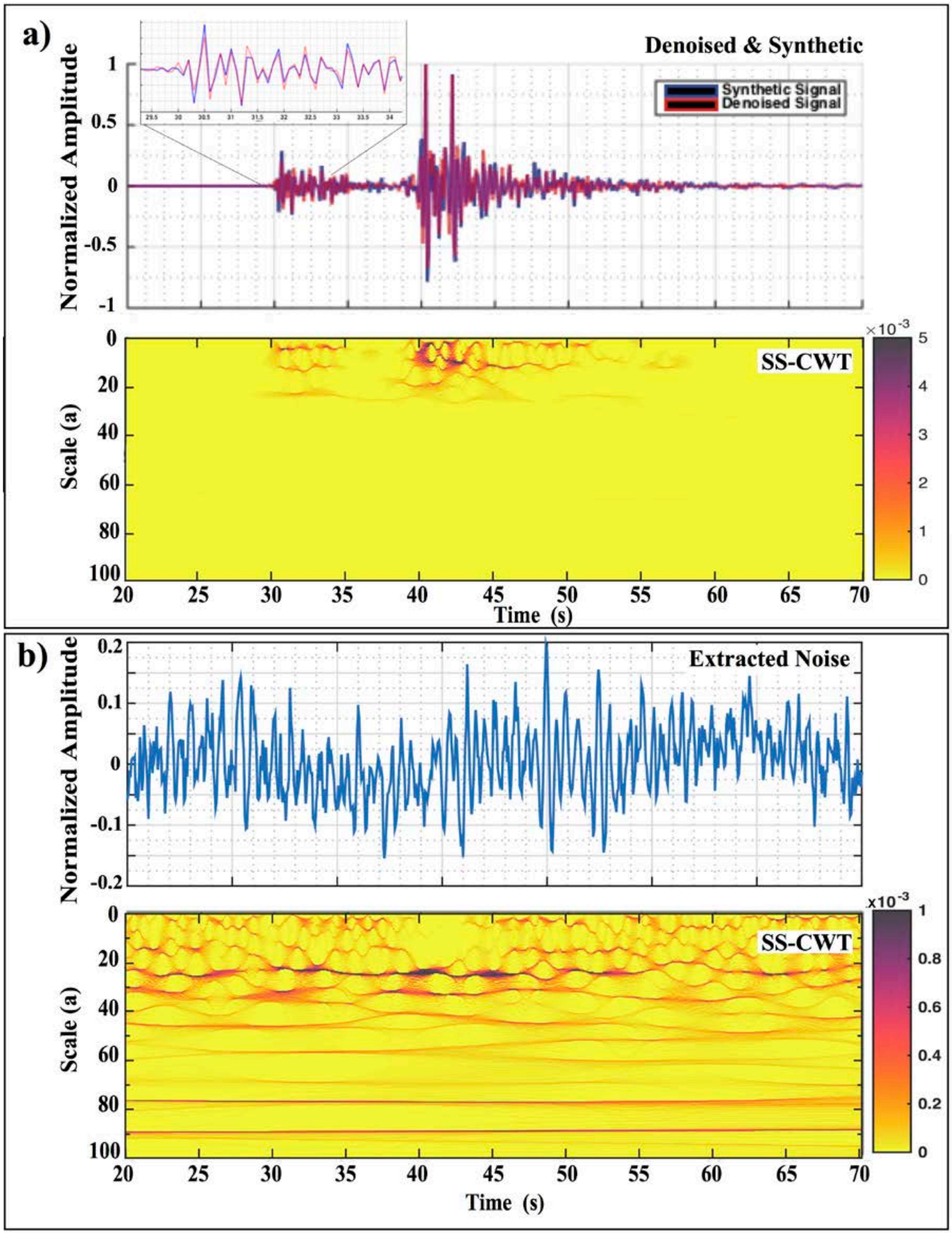

Figure 4. a) Denoised seismogram and its associated SS-CWT. b) Extracted noise and its SS-CWT found by removing the signal using a reverse approach.

Wavelet power spectra for the denoised (CWTd) and original data (CWTo) are shown in Figure 5. To compare the time-frequency structure of these two spectra we construct a cross-wavelet spectrum (XWT), which highlights regions in time-frequency space where the two spectra have high common power and represents their local relative phase (Figure 6a). To find regions where the two spectra co-vary (but do not necessarily have high power) we used wavelet squared coherency (WSC) (Figure 6b). WSC is equivalent to localized correlation in time-frequency space. The equations for XWT and WSC are given in appendix A and B, respectively.

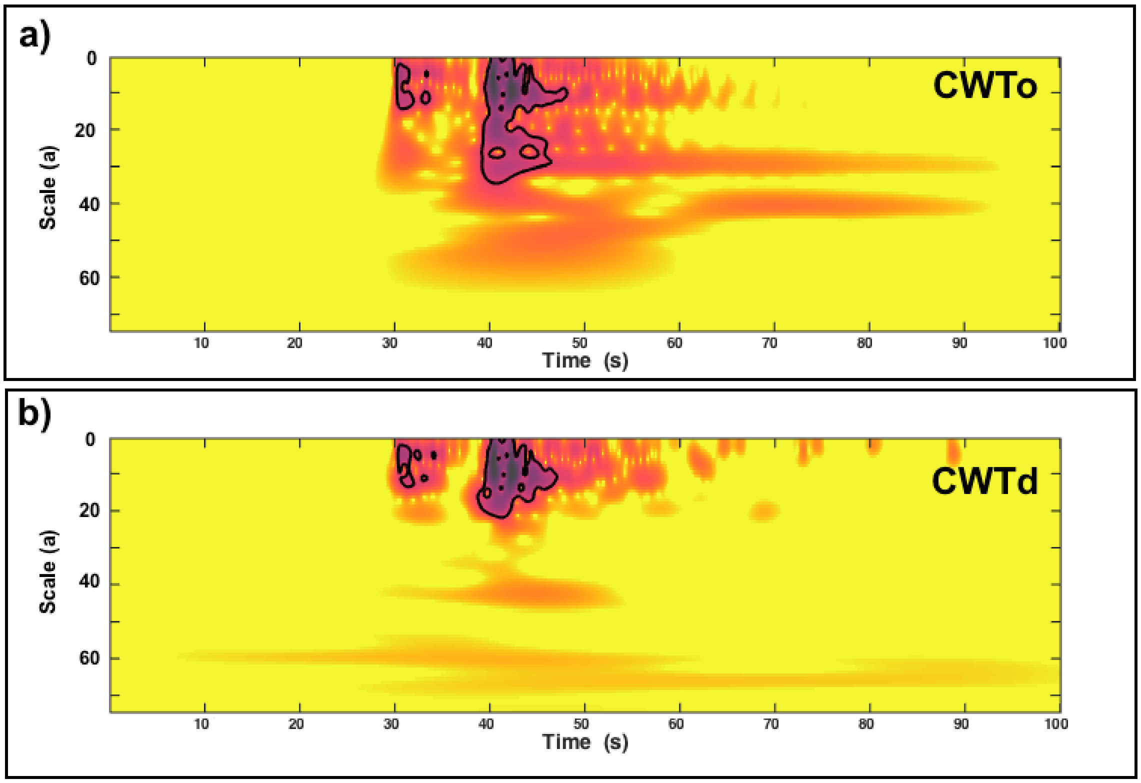

Figure 5. a) Wavelet spectrogram of synthetic data before adding noise (CWTo). b) The same for denoised data (CWTd).

High power areas in Figure 6a indicate the correlation of high magnitude coefficients in the denoised and original CWT spectrums. High-power regions within CWTo and CWTd coincide for arrival times between 30 and 40s, indicating preservation of P and S energy after denoising. The two waveforms are in-phase for all sectors with significant common power (Figure 6a) but the phase relationship becomes mostly anti-phase outside the common power areas. The cross-wavelet power indicates a strong link between the two spectra.

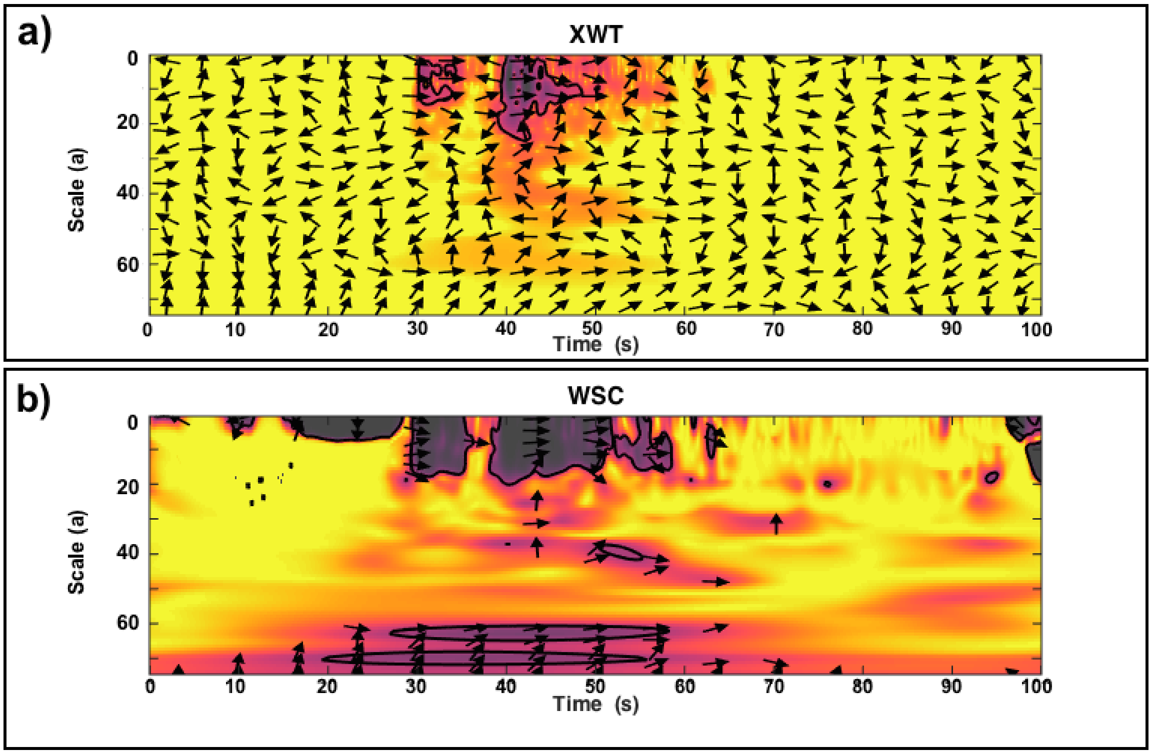

Figure 6. a) Cross-wavelet spectrum (XWT). *The XWT finds regions in time frequency space where two wavelet representations (CWTo and CWTd) show high common power. b) Wavelet squared coherency (WSC). The WTC finds regions in time frequency space where the two representations co-vary (but do not necessarily have high power).*

The WSC of denoised and original data is presented in Figure 6b. Compared with the XWT in addition to the high-power region in lower periods, a relatively large high-power section is present at higher period. An in-phase relationship exists in high-power areas. Low-power regions coincide with low wavelet powers in the original and denoised scalograms.

To investigate denoising effects on wave polarization, we perform hodogram analyses of the P-wave and S-wave windows using three component data before and after the denoising (Figure 7). The particle motions cannot be exactly the same since the amplitude of the denoised and synthetic signals do not remain the same after modification of CWT coefficients during the thresholding. However, the overall direction of motions shown by dashed lines, which represent the average of relative directions of motion for P and S, are quite similar. The relative motions (angles between dashed lines) remained approximately the same after the denoising.

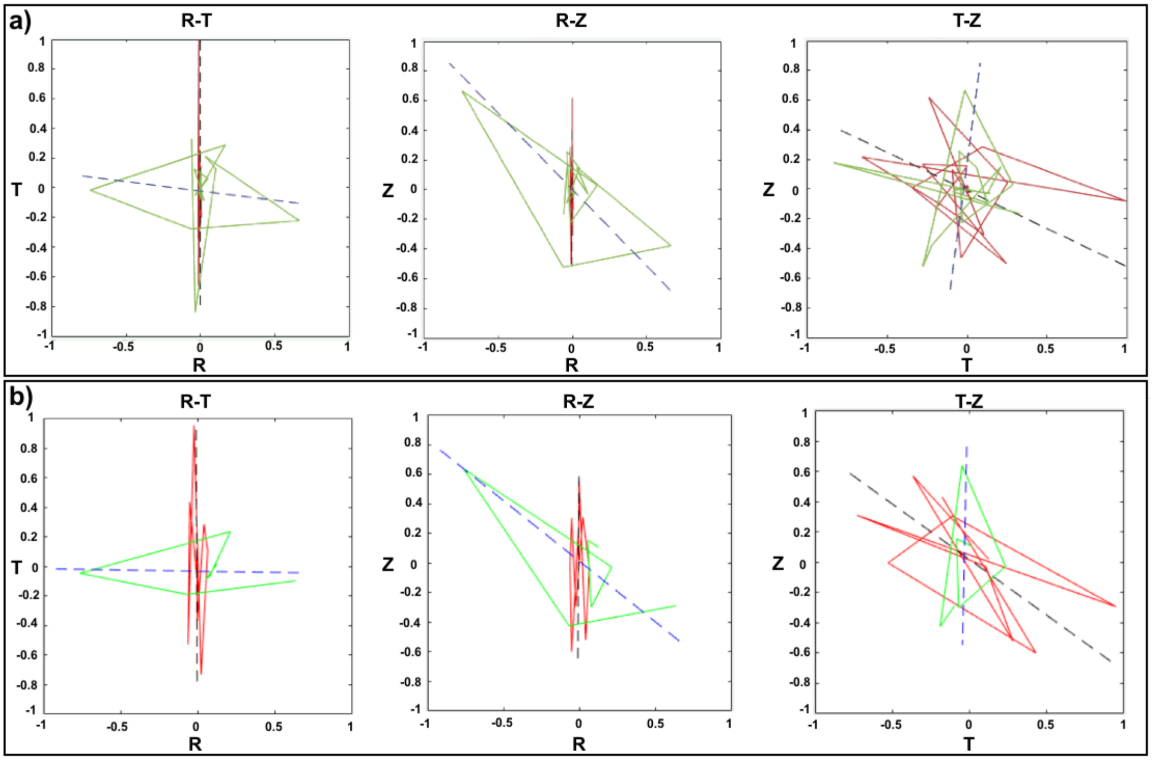

Figure 7. Hodograms for particle motion in the radial-transverse plane (R-T), radial-vertical plane (R-Z) and transverse-vertical plane (T-Z) for the synthetic seismogram without noise (a) and the processed noisy synthetic seismogram (b). *P-wave (red) and S-wave (green) are displayed. Dashed lines show the average particle motions as computed using principle component analysis. The P-wave, S-wave polarization azimuths, and the angle between P-wave and S-wave particle motions for the seismogram before the denoising are measured as 0, -79, and 94 degrees, respectively. They change to 359, -90, and 88 degrees for the denoised seismograms.*

The proposed algorithm has a better performance compared to band-pass filtering, hard-thresholding, soft-thresholding, and hybrid block-thresholding (Figure 8). Bandpass filtering removes noise with frequencies higher and lower than the signal's frequency range but noise within the same frequency range of the signal remains untouched (Figure 8b). Poor performance of soft and hard thresholding (Figure 8c and d) is due to the presence of high-power features at high scales. These high-power features can be due to either ground-roll (e.g. Chen et al., 2015), tilt (e.g. Crawford and Webb, 2000) noise in marine experiments, strong electrical noise (e.g. Castellano and van der Baan 2013), long-period-long-duration (LPLD) signals (e.g. Zoback et al. 2012; Caffagni et al. 2015; Zecevic et al. 2016) in microseismic monitoring, or very-long-period (VLP) signals in mining-induced microearthquakes (e.g. Mousavi et al. 2015) or volcano seismology. These types of features cannot be affected by either a global or level-dependent thresholding. However, their existence can affect severely the performance of denoising in removing high-frequency components of the noise. This is because that assumption of sparsity is the key point in wavelet thresholding, since the threshold level is set to separate small magnitude coefficients, which are assumed to be due to the noise, from high-power coefficients, which are assumed to be due to the signal. Thresholding uses the data itself to decide which coefficients are significant and which are not. Best results were obtained by hybrid block-thresholding (Figure 8e) and the GCV-thresholding method of this study (Figure 8f). In both methods, high-power long-period features have been removed from TFR by implementing the pre-processing step. However, GCV-thresholding obtains much higher SNR (136.17) compared to hybrid block-thresholding (42.83) in addition to higher cross correlation with the original data (0.945), lower root mean squared error (0.025), and reduced computational time (3.38 second). Moreover, fewer coda waves were attenuated in the GCV-thresholding compared to the block-thresholding method. Quantified comparisons of the proposed algorithm with other methods are presented in Table 1.

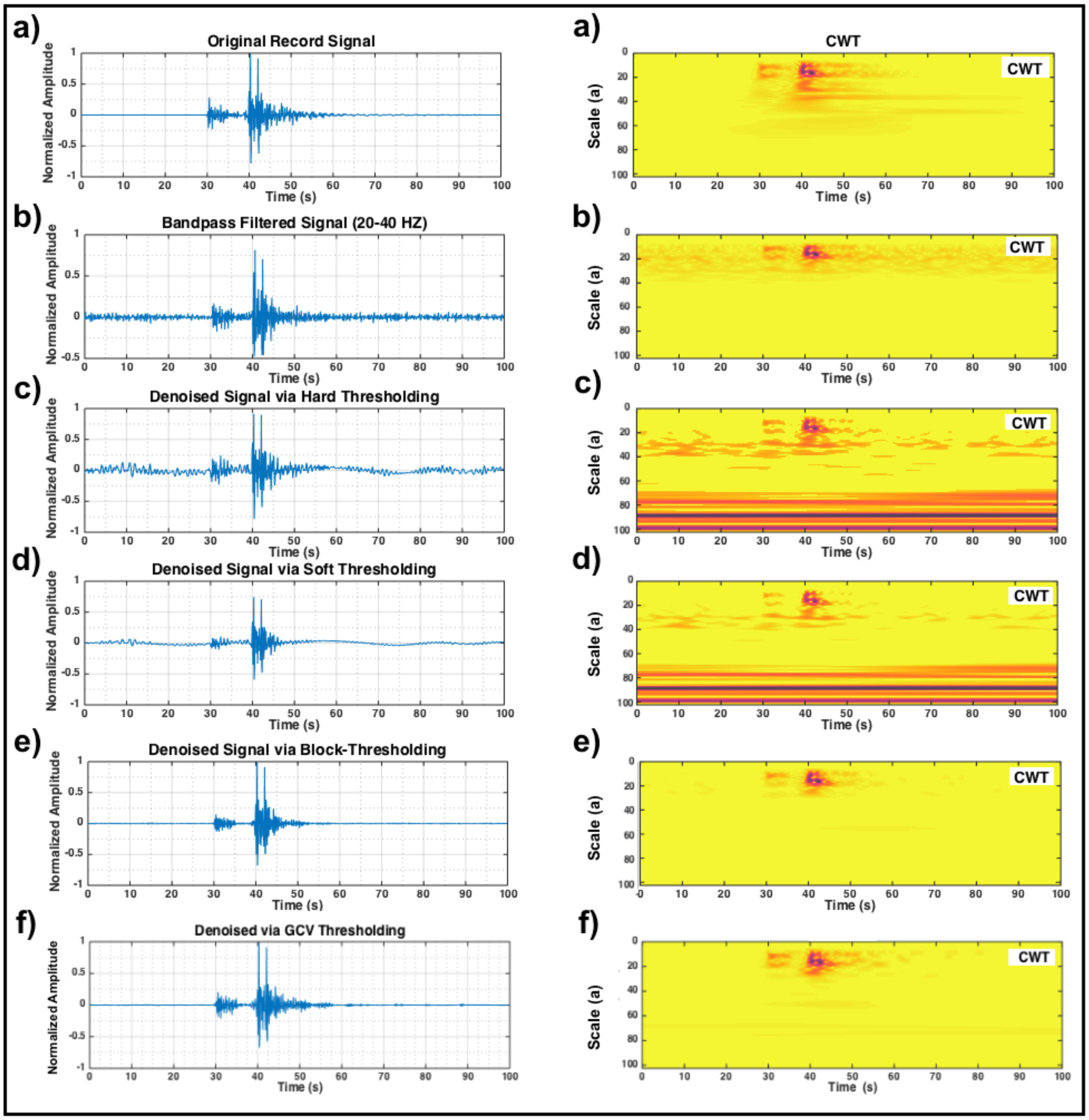

Figure 8. a) Waveforms and CWT spectrogram of synthetic data. b) *Waveforms and CWT spectrogram after band-pass filtering between 20 and 40 Hz. C) Waveforms and CWT spectrogram of data after Hard-thresholding. d) Waveforms and CWT spectrogram of data after Soft-thresholding. e) Waveforms and CWT spectrogram of data after hybrid block-thresholding. f) Waveforms and CWT spectrogram of data after denoising using the GCV-thresholding of this study.*

Table 1. Root-mean-square error (RMSE), signal-to-noise ratio (SNR), and maximum correlation coefficients between denoised and original signal (CC) from the synthetic test using bandpass filtering between 5 and 20 Hz, Hard and Soft Thresholding (Donoho and Johnston, 1994), Neighboring Thresholding (Mousavi and Langston, 2016b) and Hybrid Block-Thresholding (Mousavi and Langston, 2016a).

Method	RMSE	SNR	CC	Time (s)	TFT
Bandpass Filtering	0.063	5.441	0.683	0.19	-
Hard Thresholding	0.061	2.864	0.796	0.50	CWT
Soft Thresholding	0.048	3.457	0.833	0.51	CWT
Neighboring Thresholding	0.060	750.5	0.721	0.87	STFT
Hybrid Block-Thresholding	0.027	42.831	0.935	9.23	CWT
CGV Thresholding	0.025	136.174	0.945	3.38	SS_CWT

4.2. Field Seismic Data

Background noise is a challenging problem encountered in surface monitoring of microseismic events. We have applied the algorithm to real seismic data including two microseismic data sets induced during wastewater injection in central Arkansas (Horton 2012) and an underground collapse of a cavern in Bayou Corne, Louisiana (Mousavi et al. 2016b). Another group of seismic experiments typically known to have high background seismic-noise levels concerns seismic measurements made at the seafloor. Seismic noise at the seafloor is usually long period with frequencies below 1 Hz. Hence, we have also tested the algorithm on one M4.3 earthquake on the west coast recorded on an OBS during the Cascadia initiative experiment (Toomey et al, 2014). The selected station for OBS data (7D.FS15B) is the shallowest OBS deployed during the Cascadia initiative experiment, hence, resembling the worst-case scenario (personal comment: Andrew Barclay and Spahr Webb).

In addition to high-magnitude noise at very low frequency, some high-frequency noise components are present around scale 40 in the OBS data (Figure 9). This high-frequency noise is stronger on horizontal components. The proposed hybrid scheme was successful in attenuating coherent and high-power noise at the higher and lower scales and increasing the SNR from 2.7 to 165.5. Moreover, our method was able to automatically remove noise within the same frequency band as the signal and significantly improve the SNR for all three components. We note that the P, S, and surface waves are preserved. However, some coda are removed from S and surface waves.

In the case of the microearthquakes induced by wastewater injection (Figure 10), noise with higher and lower frequency content compared to the signal frequency was attenuated from the time-frequency representation of data with the SNR increasing from 1.3 to 303.7 (Figure 10a) and from 5.1 to 28.19 (Figure 10b). For the first event, high-energy noise components at 19, 27, 30, 33, 38, and 43 Hz were attenuated from the spectra in addition to some low frequency components. In the second example (Figure 10b), the dominant energy of the noise is concentrated between 34 and 40 Hz. The denoising algorithm improves the SNR by removing the dominant noise energy and modifying the spectral content of the signal. P and S arrivals are much clearer after denoising. This can help phase arrival time picking and improve source location estimates.

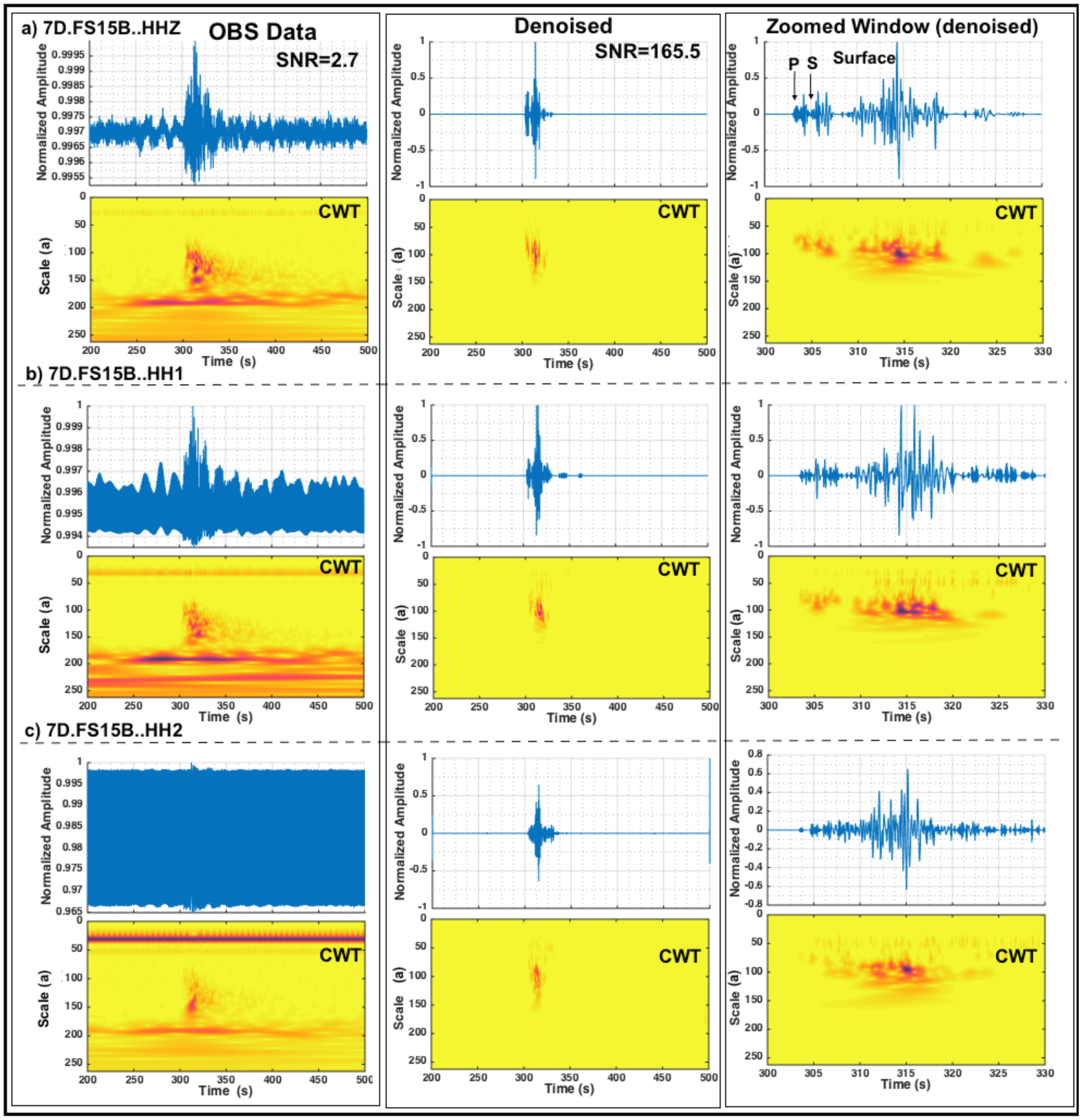

Figure 9. Denoising OBS data of M 4.3 earthquake occurring offshore of Petrolia, CA, in May 2013 recorded by an OBS (7D.FS15B) from the Cascadia initiative experiment *From left to right each column shows the original time series data and associated CWT of raw data, denoised data using proposed method, and zoomed windows around the event on denoised data respectively. a) Is the vertical and b) and c) are horizontal components of motion.*

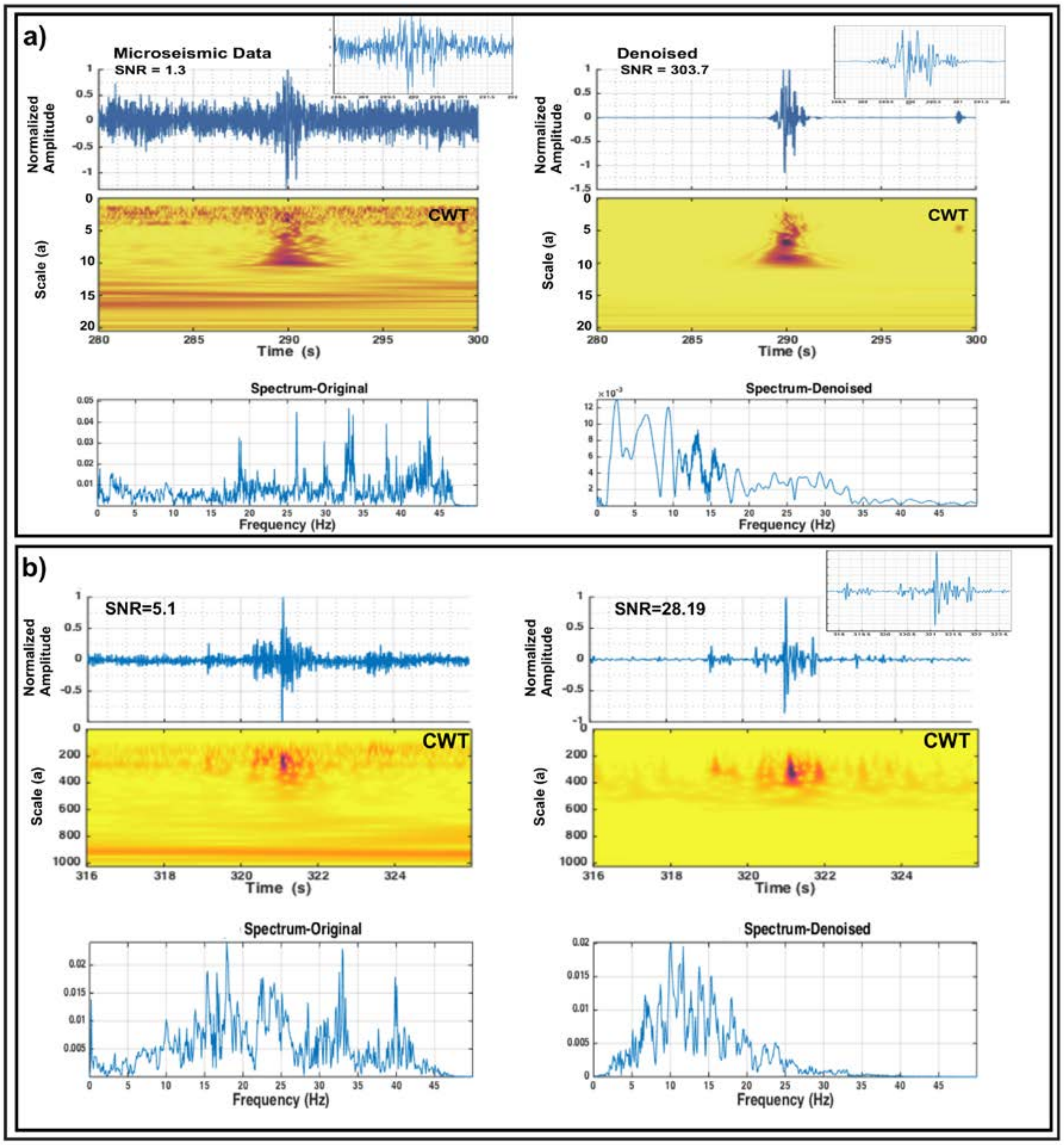

Figure 10. Denoising of two microseismic events induced by wastewater injection in central Arkansas (in 2010). *For each event (a and b) time series and associated CWT representation and a single side amplitude spectra are presented on the left and denoised results are shown on the right. There are high power bursts at 19, 27, 30, 34, 38, and 44 Hz in the spectra of raw microseismic data that could be associated with electronic noise. The proposed method removed these noises.*

Our fourth example concerns a case of mining-induced microseismic events recorded on a 7.5 minute long vertical component data trace, recorded on 1 November 2013 at Bayou Corne, Louisiana. Seven events associated with an underground collapse of a cavern can be observed on the top seismograms recorded by a three-component, 2-Hz geophone (LA17.01) at the bottom of a borehole (~287 m deep) located at 30.0134°

N, 91.1439° W (Figure 11). However, these events are not clear on other raw data (left column) recorded by two other sensors, one is a 3C broadband sensor in the same borehole near the surface (LA17.2 at ~ 190 m deep) and another a 3C broadband sensor at the surface (LA14) located at 30.0087° N, 91.1398° W (1 km south east of LA17). From the left panel in Figure 10 we can see that the noise level increases as sensors become closer to the surface. In addition to coherent and strong long period noise, some high-frequency noise exists within the surface data. SNR for the near surface data was improved after band-pass filtering between 2 and 15 Hz (middle panel in Figure 11). This is because most of the noise recorded by LA17.02 has lower-frequency compared to the microseismic events. Hence, simple spectral filtering helps to reveal most of the events that were covered by background noise. However, filtering does not improve the SNR of LA14 data because of the presence of some high-frequency noise within the same frequency band as the seismic events. In the right panel (Figure 11) the data are presented after denoising using our method. Significant improvement of the SNR occurs in all three cases indicating that our proposed method is not just limited to random noise, but is effective for removing colored noise. By applying the method on single channel data, noise that is not coherent across an array can be detected and attenuated. This SNR enhancement has special importance for microseismic detection, which is a challenging problem in surface monitoring of microseismic events. However, some isolated noise was left even after processing. Such noise can be removed by block-thresholding. Zoomed windows around each event are presented in Figure 12. Revealing the P wave arrival that was buried under background noise can facilitate the picking of first arrival times that will improve source location estimates and fracture imaging.

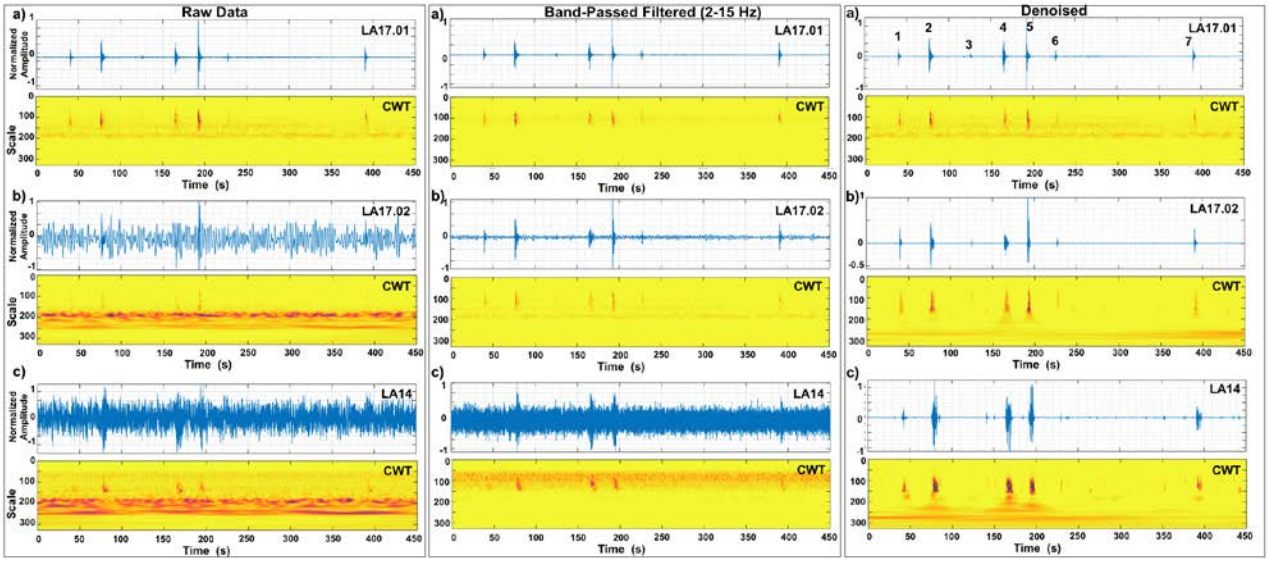

Figure 11. 7.5 minutes long vertical seismograms passively recorded in November 1st 2013 at Bayou Corne, Louisiana. a) A three-component 2-Hz geophone (LA17.01) at the bottom of a borehole (~287 m deep) located at 30.0134° N, 91.1439° W. b) A three-component broadband sensor (Trillium-compact) (LA17.02) at the top of the same borehole (~ 190 m deep). c) A three-component broadband sensor (Trillium-compact) (LA14) at the surface located at 30.0087° N, 91.1398° W (1 km south east of LA17). *The left panel are raw data recorded in these stations and their continuous wavelet transforms (CWT). 7 microearthquakes induced by underground collapse of the cavern in the area are observable on the borehole data (LA17.01), while near surface (LA17.02) and surface (LA14) data are much noisier. Middle panel are the same traces after band-pass filtering between 2 and 15 Hz. As most of the noise in LA17.02 (b) has lower-frequencies compared to microseismic events, spectral filtering helps reveal most of the events that were covered under background noise. However, filtering does not improve SNR at LA14 because of presence of some high-frequency noise within the frequency range of the seismic events. In the right panel data are presented after denoising by the proposed method of this study. Denoising is successful in removing the noise and results in significant improvement in the SNR in b and c. However, some isolated noise was left in b. Zoomed windows around each events are presented in Figure 12.*

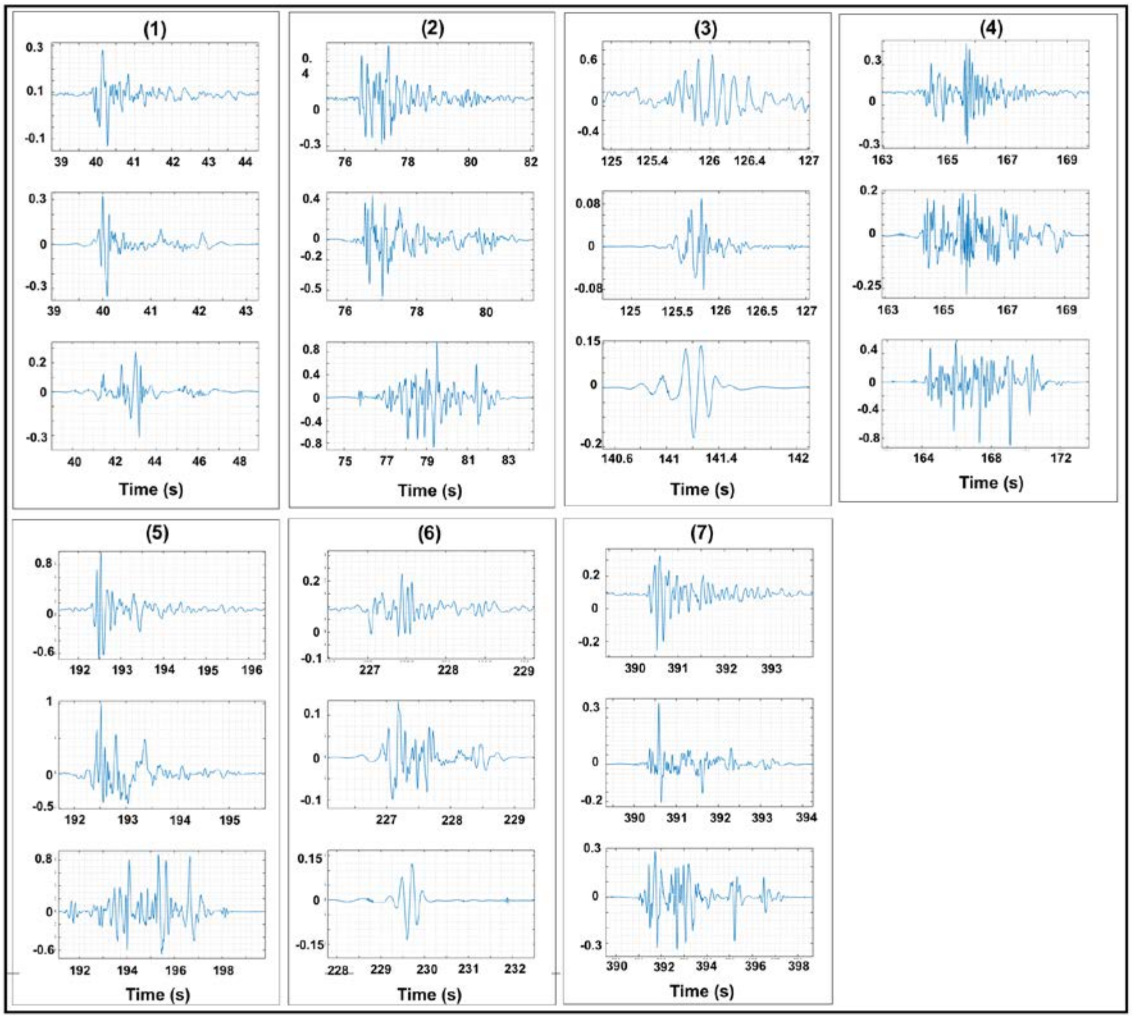

Figure 12. Zoomed windows around each microseismic events presented in continues record of Figure 11. *In each panel from top to bottom are raw data recorded on LA17.01 (bottom of the borehole), denoised data recorded on LA17.02 (same location, near the surface), and denoised data recorded on LA14 (at the surface one kilometer south-east of the LA17).*

In Figure 13 we present results of applying the algorithm in the reverse manner using the OBS and Arkansas microearthquake data to remove the signal's energy and preserve the noise. As one can see from Figure 13 the algorithm is successful in removing the signal even when it is completely buried under the background noise (Figure 13a-3).

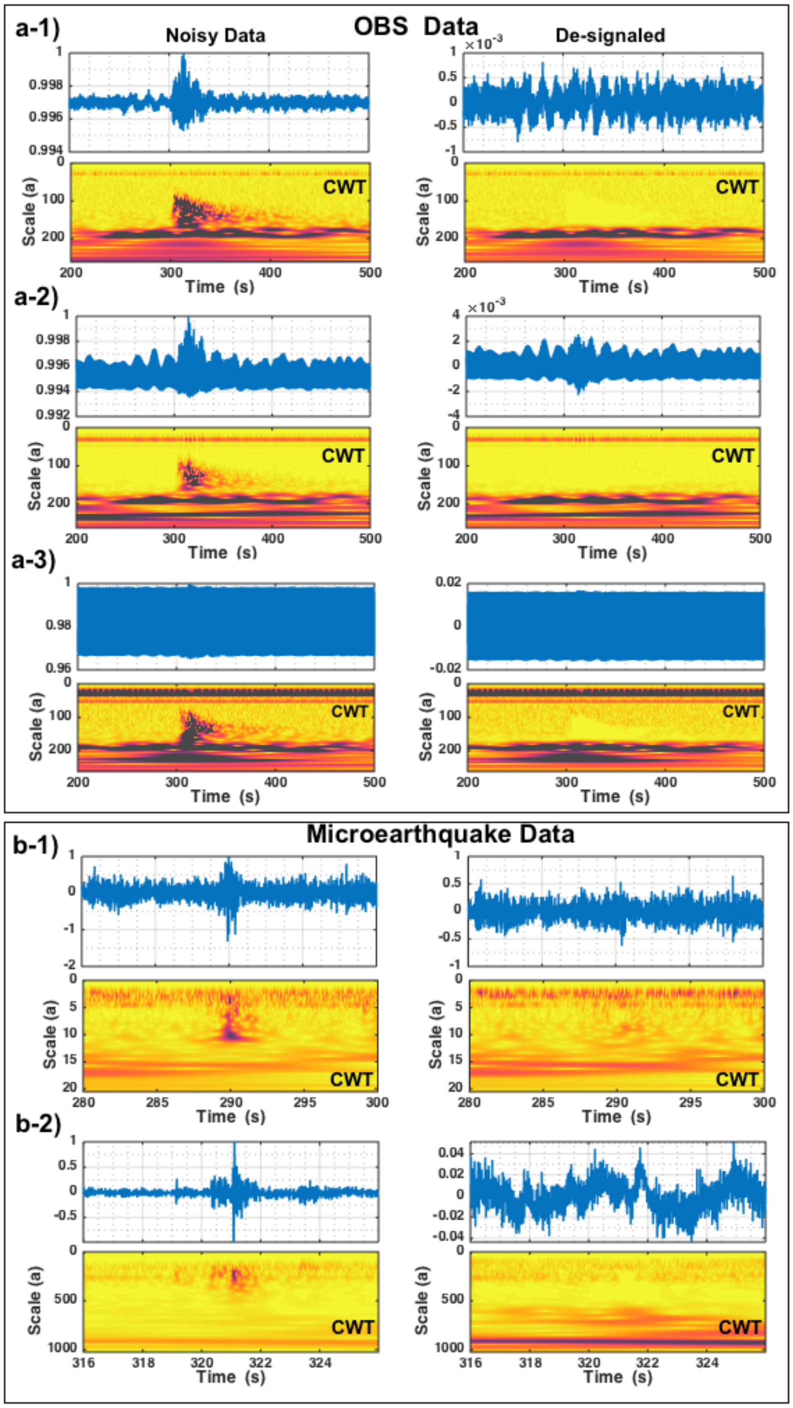

Figure 13. OBS (a) and microearthquake (b) data as presented in Figures 9 and 10. *Left column shows raw data and the right column are data after removing the signal's energy (de-signaling) from traces. As you can see the algorithm is successful in removing the signal from waveform event in the case that signal is completely buried under the background noise (Figure 13a-3) and it is hard to identify the presence of the signal and removing it using the commonly used time normalizations in ambient noise studies.*

4.3. Discussion

It is well-known that the typical background seismic noise level is much higher at the seafloor than on land, especially for frequencies below 1 Hz (e.g. Sutton and Barstow 1990; Webb et al. 1994; Romanowicz et al. 1998). Efforts have concentrated on attenuating some specific types of noise that have strong effects on the SNR of data in seafloor seismic measurements. Some examples include the proposed method of Crawford and Webb, (2000) for identifying and removing tilt noises with frequencies less than 0.1 Hz from vertical data, the proposed method of Webb (1998) for removing compliance noise from OBS data, or the proposed method of Chen et al., (2015) for attenuating ground-roll noise. The effectiveness of our hybrid algorithm for denoising OBS data has been shown in the previous section. Our proposed method is not limited to any specific type of noise but can effectively identify and then remove noise from data.

Comparing our denoising method with common methods used for microseismic denoising, the proposed method does not need coherent arrivals in an array, a master event with high SNR, or parameters that need to be tuned manually. It is adaptive to data type and can effectively attenuate the background noise through an automatic procedure. This method can be applied to single channel data more appropriately for noise that is not coherent within an array and consequently improve source detection and location, which are crucial goals in microseismic monitoring. Moreover, although the analyses performed in this study were limited to microearthquake and earthquake seismograms this method can be applied to typical reflection data. The single channel approach of this method makes it possible to combine it with other array-based denoising techniques.

In ambient noise studies, broad-band ambient noise needs to be accentuated by attenuating or removing earthquake signals that tend to dominate. This is usually done by band-pass filtering the raw data followed by a temporal normalization to reduce the effect of cross-correlating earthquakes. Time normalization is one of the most important steps in data preparation and can be done by one-bit normalization, clipping, automatic event detection and removing, running-absolute-mean normalization, or water level normalization (Bensen et al., 2007). The first three methods are based on simplified assumptions and remove a large amount of information from the waveform. The last two methods are known to be more effective but they rely on more parameters that need to be tuned for optimal performance (Bensen et al., 2007). However, the signal removal approach proposed in this paper can be an effective procedure. The data can be processed automatically with high flexibility and adaptability. It can find buried signals and remove them from the waveform without affecting the time-frequency structure of the original data. Moreover, after cross-correlation the denoising scheme can be also used to improve the SNR of recovered Green's functions. In ambient cross-correlation, the input time series are often very long. This makes it hard to recover high-fidelity signals. Baig et al., (2009) showed that time-frequency denoising of correlograms can alleviate this problem. Hence, the proposed method can be used again in a straightforward way (removing the noise from correlation results) to improve the SNR of Green's functions and making it possible to construct high-fidelity Green's functions from shorter time series. This will be the subject of a future study.

This method has many different applications. For instance, in attenuation estimation, it can assemble the spectral content of the phase of interest more precisely and decrease the uncertainties (McNamara et al., 2012; Mousavi et al., 2014; Tary et al., 2016).

5. CONCLUSIONS

We have proposed a new and fast algorithm for accurate noise-removal/signal-removal based on higher order statistics (HOS), general cross validation (GCV), and wavelet hard thresholding (WHT) in the synchrosqueezed domains. Performance of the proposed algorithm was tested using synthetic and real seismic data and showed improvements over our previous method. The denoising procedure proposed here is a powerful, data driven method that can significantly improve SNR and lower the detection threshold for small seismic events. This automatic algorithm can remove both high and low frequency seismic noise and retrieve the seismic signal with full features such as dominant phases, polarity and spectral content. The method can be used for single component data and is applicable to land and ocean bottom data processing.

REFERENCES

Ahrabian, A. and D. P. Mandic, 2015, A Class of Multivariate Denoising Algorithms Based on Synchrosqueezing, *IEEE Transactions on Signal Processing*, **63**, pp. 2196-2208, doi:10.1109/TSP.2015.2404307.

Allen, J. B. and L. R. Rabiner, 1977, A Unified Approach to Short-Time Fourier Analysis and Synthesis, *Proceedings of the IEEE*, **65,** pp. 1558-1564, doi:10.1109/PROC.1977.10770.

Auger, F., P. Flandrin, Y. T. Lin, S. McLaughlin, S. Meignen, T. Oberlin, and H. T. Wu, 2013, Time-frequency reassignment and Synchrosqueezing: an overview, *IEEE Signal Processing Magazine*, **30**, pp. 32-41, doi: 10.1109/MSP.2013.2265316.

Auger, F. and P. Flandrin, 1995, Improving the Readability of Time-Frequency and Time-Scale Representations by the Reassignment Method, *IEEE Transactions on Signal Processing*, **43,** pp. 1068-89, doi:10.1109/78.382394.

Baig, A., M. Campillo, and F. Brenguier, 2009, Denoising Seismic Noise Cross Correlations, *J. Geophys. Res*, **114**, B08310, doi:10.1029/2008JB006085.

Bekara, M. and M. van der Baan, 2009, Random and Coherent Noise Attenuation by Empirical Mode Decomposition, *Geophysics*, **74,** no. 5, pp. V89-98, doi:10.1190/1.3157244.

Bensen, G. D., M. H. Ritzwoller, M. P. Barmin, A. L. Levshin, F. Lin, M. P. Moschetti, N. M. Shapiro, and Y. Yang, 2007, Processing Seismic Ambient Noise Data to Obtain Reliable Broad-Band Surface Wave Dispersion Measurements, *Geophys. J. Int*, **169**, pp. 1239-1260.

Bickel, P. J. and K. A. Doksum, 1977, Mathematical Statistics, Holden-Day, San Francisco, CA.

Bogiatzis, P. and M. Ishii, 2015, Continuous wavelet decomposition algorithms for automatic detection of compressional- and shear-wave arrival times, *Bulletin of Seismological Society of America*, **105**, pp. 1628-1641, doi: 10.1785/0120140267.

Bonar, D. and M. D. Sacchi, 2012, Denoising seismic data using the non-local means algorithm, *Geophysics*, 77 (1), pp. A5-A8.

Caffagni, E., D. Eaton, M. van der Baan, and J. P. Jones, 2015, Regional seismicity: A potential pitfall for identification of long-period long-duration events, *Geophysics*, 80, no. 1, pp. 1-5.

Carmona, R. A., W. L. Hwang, and B. Torresani, 1997, Characterization of Signals by the Ridges of Their Wavelet Transforms: Signal Processing, IEEE Transactions, **45**, pp. 2586-2590.

Castellanos, F. and M. van der Baan, 2013, Microseismic Event Locations Using the Double-Difference Algorithm, *CSEG Recorder*, **38**, pp. 26-37.

Chassande-Mottin, E., I. Daubechies, F. Auger, and P. Flandrin, 1997, Differential Reassignment, *IEEE Signal Processing Letters*, **4** , pp. 293-294, doi:10.1109/97.633772.

Chen Y., J. Ma, S. Fomel, 2016, Double-sparsity dictionary for seismic noise attenuation, *Geophysics*, **81**, no. 2, pp. V17-V30.

Chen, Y. and J. Ma, 2014, Random Noise Attenuation by F-X Empirical Mode Decomposition Predictive Filtering, *Geophysics*, **79**, no. 3, pp. V81-91.

Chen, Y., S. Jiao, J. Ma, H. Chen, Y. Zhou, S. Gan, 2015, Ground-Roll Noise Attenuation Using a Simple and Effective Approach Based on Local Band- Limited Orthogonalization Ground-Roll Noise Attenuation Using a Simple and Effective Approach Based on Local, *IEEE Geoscience and Remote Letters,* **12**, pp. 2316-2320, doi:10.1109/LGRS.2015.2475280.

Crawford, W. C. and S. C. Webb, 2000, Identifying and Removing Tilt Noise from Low-Frequency (<0.1 Hz) Seafloor Vertical Seismic Data, *Bulletin of Seismological Society of America*, **90**, pp. 952-63.

Daubechies, I. and S. Maes, 1996, A Nonlinear Squeezing of the Continuous Wavelet Transform Based on Auditory Nerve Models, in Wavelets in Medicine and Biology, pp. 527-546, eds. A. Aldroubi and M. Unser, CRC Press, Boca Raton, FL.

Daubechies, I. and C. Heil, 1992, Ten Lectures on Wavelets, *Computers in Physics*, **6** AIP Publishing, p. 697, doi:10.1063/1.4823127.

Daubechies, I., J. Lu, and H. Tieng Wu, 2011, Synchrosqueezed Wavelet Transforms: An Empirical Mode Decomposition-like Tool, *Applied and Computational Harmonic Analysis*, **30**, pp. 243-261, doi:10.1016/j.acha.2010.08.002.

Ditommaso, R., M. Mucciarelli, M. R. Gallipoli, and F. C. Ponzo, 2010, Effect of a single vibrating building on free-field ground motion: numerical and experimental evidences, *Bull Earthquake Eng*., **8**, pp. 693-703, doi:10.1007/s10518-009-9134-5.

Ditommaso, R., M. Mucciarelli, and F. C. Ponzo, 2012, Analysis of non-stationary structural systems by using a band-variable filter, *Bull Earthquake Eng*., **10**, pp. 895-911, doi:10.1007/s10518-012-9338-y.

Donoho, D. L. and I. M. Johnstone, 1995, Adapting to Unknown Smoothness via Wavelet Shrinkage, *Journal of the American Statistical Association*, **90**, pp. 1200-1224.

Donoho, D. L. and I. M. Johnstone, 1994, Ideal Spatial Adaption by Wavelet Shrinkage, *Biometrika*, doi:10.1093/biomet/81.3.425.

Douglas, A., 1997, Bandpass Filtering to Reduce Noise on Seismograms: Is There a Better Way?, *Bulletin of Seismological Society of America,* **87,** pp. 770-777.

Farge, M., 1992, Wavelet Transforms and Their Applications to Turbulence: November, Annual Reviews, 4139 El Camino Way, P.O. Box 10139, Palo Alto, CA 94303-0139, USA, http://www.annualreviews.org/doi/abs/10.1146/annurev.fl.24.010192.002143.

Gabor, D., 1946, Theory of Communication. Part 1: The Analysis of Information, *Journal of the Institution of Electrical Engineers - Part III: Radio and Communication Engineering*, **93**, pp. 429-441, doi:10.1049/ji-3-2.1946.0074.

Galiana-Merino, J. J., J. Rosa-Herranz, J. Giner, S. Molina, and F. Botella, 2003, De-Noising of Short-Period Seismograms by Wavelet Packet Transform: *Bulletin of Seismological Society of America*, **93,** pp. 2554-1562, doi:10.1785/0120010133.

Ghael, Sandeep P., Akbar M. Sayeed, and Richard G. Baraniuk, 1997, Improved Wavelet Denoising via Empirical Wiener Filtering, *Proceedings of SPIE, Mathematical Imaging,* San Diego, CA, July, pp. 389-399, doi:10.1117/12.292799.

Gómez, J. L. and D.R. Velis, 2016, A simple method inspired by empirical mode decomposition for denoising seismic data, *Geophysics*, 81, No. 6, pp. V403-V413, doi:10.1190/GEO2015-0566.1.

Grinsted, A., J. C. Moore, and S. Jevrejeva, 2004, Application of the Cross Wavelet Transform and Wavelet Coherence to Geophysical Time Series, *Nonlinear Processes in Geophysics*, **11**, pp. 561-66, doi:10.5194/npg-11-561-2004.

Hall, M., 2006, Resolution and Uncertainty in Spectral Decomposition, First Break, **24, pp.** 43-47, doi:10.3997/1365-2397.2006027.

Han, J. and M. van der Baan, 2015, Microseismic and Seismic Denoising via Ensemble Empirical Mode Decomposition and Adaptive Thresholding, *Geophysics*, **80,** no. 6, pp. KS69-KS80, doi:10.1190/geo2014-0423.1.

Herrera, R. H., J. B. Tary, M. van der Baan, and D. W. Eaton, 2015, Body Wave Separation in the Time-Frequency Domain, *IEEE Geoscience and Remote Sensing Letters*, **12**, pp. 364-368, doi:10.1109/LGRS.2014.2342033.

Herrera, R. H., J. Han, and M. van der Baan, 2014, Applications of the Synchrosqueezing Transform in Seismic Time-Frequency Analysis, *Geophysics*, **79,** no. 3, pp. V55-64, doi:10.1190/geo2013-0204.1.

Horton, S., 2012, Disposal of hydrofracking waste fluid by injection into subsurface aquifers triggers earthquake swarm in central Arkansas with potential for damaging earthquake, *Seismological Research Letters*, **83**, pp. 250-260.

Huang, W., R. Wang, Y. Chen, H. Li, and S. Gan, 2016, Damped multichannel singular spectrum analysis for 3D random noise attenuation, *Geophysics*, **81**, no. 4, pp. V261-V270.

Huang, N. E., Z. Shen, S. R. Long, M. C. Wu, H. H. Shih, Q. Zheng, N.-C. Yen, C. C. Tung, and H. H. Liu, 1998, The Empirical Mode Decomposition and the Hilbert Spectrum for Nonlinear and Non-Stationary Time Series Analysis, *Proceedings of the Royal Society A, Mathematical, Physical and Engineering Sciences*, **454**, pp. 903-995, doi:10.1098/rspa.1998.0193.

Huang, Z. l., J. Zhang, T. H. Zhao, and Y. Sun, 2015, Synchrosqueezing S-Transform and Its Application in Seismic Spectral Decomposition, *IEEE Transactions on Geoscience and Remote Sensing*, **54**, pp. 817-825, doi:10.1109/TGRS.2015.2466660.

Iatsenko, D., P. V. E. McClintock, and A. Stefanovska, 2015, Linear and Synchrosqueezed Time-Frequency Representations Revisited: Overview, Standards of Use, Resolution, Reconstruction, Concentration, and Algorithms, *Digital Signal Processing, A Review Journal*, **42,** pp. 1-26, doi:10.1016h/j.dsp.2015.03.004.

Jansen, M., M. Malfait, and A. Bultheel, 1997, Generalized Cross Validation for Wavelet Thresholding, *Signal Processing*, **56,** pp. 33-44, doi: 10.1016/S0165-1684(97)83621-3.

Johnstone, I. M. and B.W. Silverman, 1997, Wavelet Threshold Estimators for Data with Correlated Noise, *Journal of the Royal Statistical Society*, **59**, pp. 319-51.

Karamzadeh, N., G. J. Doloei, and A. Reza, 2013, Automatic earthquake signal onset picking based on the continuous wavelet transform, *IEEE Transactions on Geoscience and Remote Sensing*, **51**, pp. 2666-2674, doi: 10.1109/TGRS.2012.2213824.

Li H., R. Wang, S. Cao, Y. Chen, W. Huang, 2016, A method for low-frequency noise suppression based on mathematical morphology in microseismic monitoring, *Geophysics* **81**, no. 3, pp. V159-V167.

Mallat, S., 1999, A wavelet tour of signal processing, in wavelet analysis and Its applications, Second Ed., Academic Press, San Diego, CA.

McNamara, D., M. Meremonte, J. Z. Maharrey, S.-L. Mildore, J. R. Altidore, D. Anglade, S. E. Hough, D. Given, H. Benz, L. Gee, and A. Frankel, 2012, Frequency-dependent seismic attenuation within the Hispaniola Island region of the Caribbean Sea, *Bull. Seismol. Soc. Am*., **102**, p. 773-782.

Meignen, S., T. Oberlin, and S. McLaughlin, 2012, A New Algorithm for Synchrosqueezing: With an Application to Multicomponent Signals Sampling and Denoising, *IEEE Transactions on Signal Processing*, **60**, pp. 5787-5798.

Mousavi, S. M., C. A. Langston, and S. P. Horton, 2016a, Automatic Microseismic Denoising and Onset Detection Using the Synchrosqueezed-Continuous Wavelet Transform, *Geophysics*, **81**, no. 4, pp. 1-15, doi:10.1190/GEO2015-0598.1.

Mousavi, S. M., S. P. Horton, C. A. Langston, and B. Samei, 2016b, Seismic features and automatic discrimination of deep and shallow induced-microearthquakes using neural network and logistic regression, *Geophys. J. Int*., 207, pp. 29-46, doi:10.1093/gji/ggw258.

Mousavi, S. M. and C. A. Langston, 2016a, Hybrid Seismic Denoising Using Higher-Order Statistics and Improved Wavelet Block Thresholding, *Bulletin of Seismological Society of America*, 106, doi:10.1785/0120150345.

Mousavi, S. M. and C. A. Langston, 2016b, Adaptive noise estimation and suppression for improving microseismic event detection, *Journal of Applied Geophysics*, 132, pp. 116-124, http://dx.doi.org/10.1016/j.jappgeo.2016.06.008.

Mousavi, S. M. and C. A. Langston, 2016c, Fast and novel microseismic detection using time-frequency analysis, *SEG Technical Program Expanded Abstracts*, pp. 2632-2626, doi:10.1190/segam2016-13262278.

Mousavi, S. M., S. P. Horton, and C. L. Langston, 2015, Differences Between Locations from Surface Seismometers and Downhole Geophones at the Napoleonville Salt Dome Louisiana, In *SSA Annual Meeting 2015*, Pasadena, CA.

Mousavi, S. M., C. H. Cramer, and C. A. Langston, 2014, Average QLg, QSn, and observation of Lg blockage in the continental Margin of Nova Scotia, *J. Geophys. Res*. 119, pp. 7722-7744, doi:10.1002/2014JB011237.

Naghizadeh, M. and M. Sacchi, 2012, Multicomponent Seismic Random Noise Attenuation via Vector Autoregressive Operators, *Geophysics*, **77**, no. 2, pp. V91-99, doi:10.1190/geo2011-0198.1.

Naghizadeh, M., 2011, Seismic Data Interpolation and Denoising in the Frequency-Wavenumber Domain, *Geophysics*, **77**, no. 2, pp. V71-V80, doi: 10.1190/GEO2011-0172.1.

Nason, G. P., 1996, Wavelet Shrinkage Using Cross-Validation, *Journal of the Royal Statistical Society, Series B (Methodological)*, **58,** pp. 463-479, http://citeseerx.ist.psu.edu/viewdoc/summary?doi=10.1.1.144.5690.

Oropeza, V. and M. Sacchi, 2011, Simultaneous seismic data denoising and reconstruction via multichannel singular spectrum analysis, *Geophysics*, **76**, no. 3, pp. V25-V32.

Parolai S., 2009, Denoising of Seismograms Using the S Transform, *Bulletin of Seismological Society of America*, **99**, pp. 226-234, doi: 10.1785/0120080001.

Pazos, A., M. J. Gonz, and G. Alguacil, 2003, Non-Linear Filter, Using the Wavelet Transform, Applied to Seismological Records, *Journal of Seismology*, **7**, pp. 413-429.

Pinnegar, C. R. and D. W. Eaton, 2003, Application of the S transform to prestack noise attenuation filtering, *J. Geophys. Res.*, 108, p. 2422, doi:10.1029/2002JB002258.

Ravier, P. and P. O. Amblard, 2001, Wavelet Packets and Denoising Based on Higher-Order-Statistics for Transient Detection, *Signal Processing*, **81**, pp. 1909-1926.

Reine, C., M. van der Baan, and R. Clark, 2009, The Robustness of Seismic Attenuation Measurements Using Fixed- and Variable-Window Time-Frequency Transforms, *Geophysics*, **74**, no. 2, pp. WA123-WA135, doi:10.1190/1.3043726.

Romanowicz, B., D. Stakes, J. P. Montagner, P. Tarits, R. Urhammer, M. Begnaud, E. Stutzmann, 1998, MOISE: A Pilot Experiment towards Long Term Sea-Floor Geophysical Observatories, *Earth Planets Space*, **50**, pp. 927-937.

Sabbione, J. I., M. D. Sacchi, D. R. Velis, 2013, Microseismic Data Denoising via an Apex-Shifted Hyperbolic Radon Transform, *SEG Annual Meeting*, 22-27 September, Houston, TX.

Sabbione, J. I., M. D. Sacchi, D. R. Velis, 2015, Radon transform-based microseismic event detection and signal-to-noise ratio enhancement, *Journal of Applied Geophysics*, 113, pp. 51-63.

Scherbaum, F, 2001, Of Poles and Zeros: Fundamentals of Digital Seismology: January, Kluwer Academic Publishers, http://dl.acm.org/citation.cfm?id=517106.

Schimmel, M. and J. Gallart, 2007, Frequency-Dependent Phase Coherence for Noise Suppression in Seismic Array Data, *Journal of Geophysical Research: Solid Earth*, **112**, pp. 1-14, doi:10.1029/2006JB004680.

Shuchong, L. and C. Xun, 2014, Seismic Signals Wavelet Packet de-Noising Method Based on Improved Threshold Function and Adaptive Threshold, *Computer Modeling and New Technologies*, **18**, pp. 1291-1296.

Sobolev, G. and A. Lyubushin, 2006, Microseismic impulses as earthquake precursors: Izvestiya, *Physics of the Solid Earth*, **42**, pp. 721-733, doi: 10.1134/S1069351306090023.

Sutton, G. H. and N. Barstow, 1990, Ocean Bottom Ultra-Low Frequency (ULF) Seismo-Acoustic Ambient Noise: 0.002–0.4 Hz, *J. Acoust. Soc. Am*, **87**, pp. 2005-2012.

Tary, J. B., M. van der Baan, and R.H. Herrera, 2016. Attenuation Estimation Using High Resolution Time-Frequency Transforms, *Digital Signal Processing*, 60, pp. 46-55, doi:10.1016/j.dsp.2016.08.007.

Tary, J. B., R. H. Herrera, J. Han, and M. van der Baan, 2014, Spectral estimation—What Is New? What Is Next?, *Reviews of Geophysics*, **52**, pp. 723-749. doi:10.1002/2014RG000461.

Thakur, G. and H. T. Wu, 2011, Synchrosqueezing-Based Recovery of Instantaneous Frequency from Nonuniform Samples, *SIAM Journal on Mathematical Analysis*, **43**, pp. 2078-2095, doi:10.1137/100798818.

Thakur, G., E. Brevdo, N. S. Fučkar, and H. T. Wu, 2013, The Synchrosqueezing Algorithm for Time-Varying Spectral Analysis: Robustness Properties and New Paleoclimate Applications, *Signal Processing*, **93**, pp. 1079-1094, doi:10.1016/j.sigpro.2012.11.029.

Toomey, D.R., R.M. Allen, A.H. Barclay, S.W. Bell, P.D. Bromirski, R.L. Carlson, X. Chen, J.A. Collins, R.P. Dziak, B. Evers, D.W. Forsyth, P. Gerstoft, E.E.E. Hooft, D. Livelybrooks, J.A. Lodewyk, D.S. Luther, J.J. McGuire, S.Y. Schwartz, M. Tolstoy, A.M. Tréhu, M. Weirathmueller, and W.S.D. Wilcock, 2014, The Cascadia Initiative: A sea change in seismological studies of subduction zones, *Oceanography* 27(2), pp.138-150, http://dx.doi.org/10.5670/oceanog.2014.49.

Torrence, C. and G. F. Compo, 1998, A Practical Guide to Wavelet Analysis, *Bull. Am. Meteorol. Soc*., **79,** pp. 61-78.

Torrence, C. and P. Webster, 1999, Interdecadal Changes in the ESNOMonsoon System, *J. Clim*, **12**, pp. 2679-2690.

Tselentis, G. A., N. Martakis, P. Paraskevopoulos, A. Lois, and E. Sokos, 2012, Strategy for Automated Analysis of Passive Microseismic Data Based on S-Transform, Otsu's Thresholding, and Higher Order Statistics, *Geophysics*, **77**, no. 6, p. KS43, doi:10.1190/geo2011-0301.1.

Velis, D., J. I. Sabbione, and M. D. Sacchi, 2015, Fast and automatic microseismic phase-arrival detection and denoising by pattern recognition and reduced-rank filtering, *Geophysics*, 80, no. 6, pp. WC25-WC38, doi:10.1190/GEO2014-0561.1

Webb, S. C., W. C. Crawford, and J. A. Hildebrand, 1994, Long Period Seismometer Deployed at OSN-1, *OSN Newsletter, Seismic Waves*, **3**, pp. 4-6.

Webb, S. C., 1998, Broadband seismology and noise under the ocean, *Reviews of Geophysics*, 36, pp. 105-142, doi: 10.1029/97RG02287.

Weyrich, N, and G. Warhola, 1995, De-Noising Using Wavelets and Cross Validation, *Journal of Approximation Theory,* doi:10.1007/978-94-015-8577-4_36.

Yang, H., 2015, Synchrosqueezed Wave Packet Transforms and Diffeomorphism Based Spectral Analysis for 1D General Mode Decompositions, *Applied and Computational Harmonic Analysis*, **39**, pp. 33-66, doi:10.1016/j.acha.2014.08.004.

Yang, H. and L. Ying, 2014, Synchrosqueezed Curvelet Transform for Two-Dimensional Mode Decomposition, *The SIAM Journal on Mathematical Analysis*, **46**, pp. 2052-2083.

Zecevic, M., G. Daniel, and D. Jurick, 2016, On the nature of long-period long-duration seismic events detected during hydraulic fracturing, *Geophysics*, 81(3), pp. KS113-KS121.

Zhang, L., Y. Wang, Y. Zheng, and X. Chang, 2015, Deblending using a high-resolution radon transform in a common midpoint domain, *J. Geophys. Eng*., 12, pp. 167-174.

Zhu, L. and L. A. Rivera, 2002, A note on the dynamic and static displacements from a point source in multi-layered media, *Geophys. J. Int*., 148, pp. 619-627.

Zoback, M. D, A. Kohli, I. Das, and M. Mcclure, 2012, The Importance of Slow Slip on Faults During Hydraulic Fracturing Stimulation of Shale Gas Reservoirs, no. 2011, *SPE* 155476, doi:10.2118/155476-MS.

APPENDIX A

The XWT is constructed from the wavelet coefficients of the original signal (CWT_o) and the denoised signal (CWT_d) and will expose their common power and relative phase in time-frequency space. The XWT measures the similarity of the wavelet representations of two signals and provides the ability to account for temporal (or spatial) variability in spectral character. Following (Torrence and Compo 1998) the cross-wavelet transform is defined as:

$$XWT_{o,d} = CWT_o \times CWT_d^{*} \qquad \text{(A-1)}$$

where * denotes complex conjugation. The cross-wavelet power is defined as $|XWT_{a,d}|$, and the complex argument $arg(XWT_{a,d})$ can be interpreted as the local relative phase between denoised and original seismograms (Grinsted et al. 2004).

APPENDIX B

The coherency between two CWTs can be measured by wavelet coherency. The wavelet squared coherency is defined as the absolute value squared of the smoothed cross-wavelet spectrum, normalized by the smoothed wavelet power spectra: (Torrence and Webster 1999)

$$R^2(a) = \frac{\left|\left\langle a^{-1} XWT(a) \right\rangle\right|^2}{\left\langle a^{-1} \left|CWT_o(a)\right|^2 \right\rangle \left\langle a^{-1} \left|CWT_d(a)\right|^2 \right\rangle} \quad , \qquad \text{(B-1)}$$

where $\langle . \rangle$ indicates smoothing in both time and scale. The factor a^{-1} is used to convert to an energy density. The wavelet-coherency phase difference is given by:

$$\phi = \tan^{-1}\left(\frac{\Im\{\langle a^{-1} XWT \rangle\}}{\Re\{\langle a^{-1} XWT \rangle\}} \right) \quad , \qquad \text{(B-2)}$$

where $\Im$ is smoothed imaginary part and $\Re$ is smoothed real part of cross-wavelet coefficients. The smoothing is done using a weighted running average (or convolution) in both the scale and time. The time smoothing uses a filter given by the absolute value of the wavelet coefficient at each scale, normalized to have a total weight of unity. For the Morlet mother wavelet this is just a Gaussian $\exp(-t^2/(2a^2))$. For scale smoothing of the Morlet wavelet a boxcar filter of width $\delta j_0 = 0.60$ (from Torrence and Webster, 1999) was used.

List of Symbols, Abbreviations, and Acronyms

AFRL	Air Force Research Laboratory
AFSPC	Air Force Space Command
AFTAC	Air Force Technical Applications Center
BT	Block Thresholding
CC	Correlation Coefficient
CWT	Continuous Wavelet Transform
EMD	Empirical Mode Decomposition
GCV	General Cross Validation Thresholding
HOS	Higher Order Statistics
IMF	Intrinsic Mode Function
NLM	Non Local Means
OBS	Ocean Bottom Seismometer
RMSE	Root-mean-square error
SNR	Signal to Noise Ratio
SS	Synchrosqueezing
SS-CWT	Synchrosqueezed Continuous Wavelet Transform
STFT	Short Time Fourier Transform
TFR	Time-Frequency Representation
WHT	Wavelet Hard Thresholding
WSC	Wavelet Squared Coherency
XWT	Cross Wavelet Spectrum

DISTRIBUTION LIST

DTIC/OCP 8725 John J. Kingman Rd, Suite 0944 Ft Belvoir, VA 22060-6218	1 cy
AFRL/RVIL Kirtland AFB, NM 87117-5776	1 cy
Official Record Copy AFRL/RVBYE/Dr. Frederick Schult	1 cy

This page is intentionally left blank.